the expression of α-synuclein between excitatory and inhibitory neurons. We also examined activity-dependent synaptic vesicular recycling following treatment with high potassium. A recent report demonstrated that preformed fibrils generated by recombinant α-synuclein can promote the formation of LB-like aggregates containing endogenous α-synuclein [17]. We also treated cells with these preformed fibrils, and explored whether aggregate formation depends on the expression level of endogenous α-synuclein. Finally, we examined the expression of α-synuclein in the mouse hippocampus *in vivo* and confirmed the observations of differential expression found *in vitro*.

Materials and Methods

Animals

C57BL/6N mice were used, and all experimental designs and procedures were approved by the Committee for Animal Research, Kyoto Prefectural University of Medicine (M23-241), Kyoto Japan, and followed the guidelines of the Ministry of Education, Culture, Sports, Science, and Technology of Japan.

Antibodies

For α-synuclein detection, mouse monoclonal antibody Syn-1 (BD Biosciences, San Diego, CA, USA) and rabbit polyclonal antibody C-20 (Santa Cruz Biotechnology, Dallas, TX, USA) were used. For specific detection of human α-synuclein, mouse monoclonal antibody Syn211 (Thermo Fisher Scientific, UK) was used, because Syn211 recognizes human α-synuclein, but not mouse α-synuclein [18]. Phosphorylated α-synuclein was detected by mouse monoclonal antibody pSyn#64 (Wako Pure Chemical Industries, Japan) or rabbit polyclonal antibody phospho-S129 (Abcam, UK). Glutamic acid decarboxylase (GAD) was detected by rabbit polyclonal antibodies purchased from Sigma-Aldrich (St Louis, MO, USA). Anti-synapsin antibody was produced as previously described [19]. The following antibodies were purchased from these manufacturers: anti-synaptotagmin (Developmental Studies Hybridoma Bank, Iowa city, IA, USA), anti-vesicular glutamate transporter-1 (vGluT-1; Millipore, Billerica, MA, USA), anti-parvalbumin (Sigma-Aldrich), anti-somatostatin (Millipore), and anti-NeuN (Millipore).

Cell culture and transfection

Dissociated cells prepared from hippocampi of mouse embryos (E16-18) were disseminated onto polyethylimine coated coverslips and cultured in Neurobasal medium (Gibco, Life Technologies, Carlsbad, CA, USA) supplemented with B-27 (Gibco), L-glutamine (Nacalai Tesque, Kyoto, Japan) and penicillin/streptomycin (Nacalai Tesque). In the occasion of neuronal culture without glial cells, cells cultured for 2 days were treated with a medium containing cytosine arabinoside (AraC, 10 μM) (Sigma-Aldrich) for 12 h, followed by replacement with a complete medium. Half of the volume of medium was changed every 4 days. Unless specifically mentioned, cells were cultured without AraC treatment and most experiments were performed at 16–22 days *in vitro*.

To form intracellular aggregates containing human α-synuclein, transfection of plasmid DNA for the expression of human α-synuclein was performed using the electroporator CUY21Pro-Vitro (Nepagene, Chiba, Japan) in accordance with the manufacturer's protocol. After transfection, cells were disseminated onto coverslips. For depolarizing the neuronal cell membrane, cultured cells were treated with fresh medium containing 100 mM potassium chloride for 30 min. After depolarization, cells were treated with original complete medium for 10 min, to analyze the recovery of the cell membrane.

Immunocytochemistry

Cells were fixed with 2% paraformaldehyde (PFA) in culture medium for 10 min at room temperature. The fixed cells were permeabilized with 0.1% Triton X-100 in phosphate-buffered saline (PBS, pH 7.4) for 10 min, and blocked with 5% normal goat serum (NGS) in PBS for 30 min. Cells were then incubated with primary antibody in the blocking solution for 1–2 h. Cells were then washed with PBS and treated with a secondary antibody. For double staining, this staining procedure was repeated. The primary antibodies were detected with Alexa488- and Alexa594-conjugated secondary antibodies (Molecular Probes, Life Technologies, Carlsbad, CA, USA). For detection of the primary antibody produced in guinea pig, a fluorescein isothiocyanate-conjugated secondary antibody (Vector Laboratories, Burlingame, CA, USA) was used. Cells were washed with PBS and then with milliQ water (Millipore), and mounted with FluorSave (Millipore). Images were acquired as Z stacks (20–30 z-sections, 0.3–0.5 μm apart, 1024×1024 pixels) using a Plan-Apochromat 63x/1.40 Oil DIC objective (Carl Zeiss, Oberkochen, Germany) with an inverted laser-scanning confocal microscope, LSM510 (Carl Zeiss).

Formation of intracellular aggregates of α-synuclein

Neurons containing intracellular aggregates of α-synuclein were obtained using previously described methods [17]. Briefly, following sonication, preformed fibrils prepared from human or mouse α-synuclein were suspended in culture medium, and the final concentration was adjusted to 5 μg/ml. Cultured cells were treated with complete medium containing the fibrils for 7 days.

Fibril preparation

For preparation of recombinant human and mouse α-synuclein from bacterial culture, plasmid vectors were constructed as described previously (Tatebe et al., 2010; Watanabe et al., 2012). Briefly, PCR fragments of human and mouse α-synuclein were inserted into pTrc-His-TOPO vector (Invitrogen, Life Technologies, Carlsbad, CA, USA). Recombinant α-synuclein with a His-tag was purified by His-Accept column (Nacalai Tesque) [20,21]. Purified protein was electrophoresed and the protein band was stained by Coomassie Brilliant Blue and the purity confirmed by SDS-PAGE. Fibril forms of α-synuclein were prepared in accordance with a previous report [17] with slight modifications. Briefly, fibrils of α-synuclein were generated by incubating purified α-synuclein in PBS (final solution 2 mg/ml) at 37°C with constant agitation for 7 days. After agitation, the solution containing fibrils was ultracentrifuged at 200,000×g for 2 h. Fibrils were recovered as a precipitate at the bottom of the centrifuge tube. The resulting pellet was dissolved in the original volume of PBS and stored at −20°C until use. The supernatant was also stored. Each sample was then subjected to western blot analysis.

Construction of plasmid vector

For expression of human α-synuclein in cultured neurons, α-synuclein was amplified from a human cDNA library with the primers 5′-CGCCACCATGGATGTATTCATGAAA-3′ and 5′-GATATCTTAGGCTTCAGGTTCGTAG-3′. The PCR fragment was digested with *NotI* and then inserted into the *NotI-EcoRV* site of the pcDNA3.1/myc-HisB vector. The vector was then sequenced for confirmation.

SDS-PAGE and western blotting

Samples were denatured by heating with SDS-sample buffer (62.5 mM Tris-HCl, pH 6.8, 2% sodium dodecyl sulfate, 0.003% Pyronin Y, and 10% glycerol) containing 1% 2-mercaptoethanol at 98°C for 3 min. Proteins were separated by 15% polyacrylamide gel, and transferred to polyvinylidenedifluoride membranes (Bio-Rad Laboratories, Hercules, CA, USA). Membranes were blocked with 5% skim milk in Tris-buffered saline (TBS, pH 7.4) containing 0.1% Tween-20 for 1 h at room temperature. After treatment with primary antibody, the membrane was incubated with alkaline phosphatase-conjugated secondary antibodies. Protein bands were detected using the NBT-BCIP system (NacalaiTesque).

Image processing

The digital images obtained on the LSM510 were processed using Adobe Photoshop 7.0. Projections of Z stack images were processed with LSM Image Browser (Carl Zeiss).

Quantitative analysis

For quantification of the ratio of α-synuclein-expressing cells or aggregate-containing GAD-positive cells, two independent cell cultures were performed and three coverslips per culture were subjected to the immunocytochemical procedures. Endogenous α-synuclein and its aggregates were detected by Syn-1 and pSyn#64 antibodies, respectively. GAD-positive cell bodies (more than 75 cells per coverslip) were subjected to the cell counting procedure. For quantification of the ratio of GAD-positive cells having intracellular aggregates composed of transfected human α-synuclein, two coverslips per culture were subjected to the immunocytochemical procedures. Human α-synuclein was detected by the Syn211 antibody, followed by counting the number of GAD-positive neurons harboring human α-synuclein aggregates. These experiments were independently repeated twice. Data represent mean ± SEM. Statistical significance of the difference in the ratio of intracellular aggregate formation was analyzed using Graphpad Prism 5 with an unpaired, two-tailed Student's t test with or without Welch's correction.

After acquisition of the confocal images, quantitative colocalization analysis using Pearson's correlation test was performed (LSM Image Browser, Carl Zeiss).

Immunohistochemistry

Under deep anesthesia with pentobarbital, adult mice were intracardially perfused with PBS followed by 4% PFA in PBS. Brains were dissected into blocks including the cerebral cortex and hippocampus, and post-fixed with the same fixative for 12 h at 4°C. Coronal sections (40 μm) were obtained using a vibratome (DSK, Kyoto, Japan). Sections were permeabilized with 0.3% Triton X-100 in PBS (PBST) for 1 h, and blocked with 10% NGS in PBST for 6 h. Sections were then treated with primary and secondary antibodies following the immunocytochemical procedures described above. After these treatments, the sections were washed with PBST and then with 20 mM Tris-HCl buffer, and mounted with FluorSave. Images were acquired as Z stacks (10–20 z-sections, 1 μm apart, 1024×1024 pixels) using a Plan-Apochromat 63x/1.40 Oil DIC objective with an inverted laser-scanning confocal microscope, LSM510.

Results

Inhibitory neurons showed low expression of α-synuclein *in vitro*

Immunocytochemistry of cultured hippocampal neurons showed that α-synuclein was present in a punctate distribution, with an intense signal observed in the cell body and nucleus of some neurons (Fig. 1A). However, other neurons were unstained with either monoclonal or polyclonal antibodies against α-synuclein (Fig. 1 and Fig. S1A). There were clearly differential expression patterns of α-synuclein in cultured neurons. To characterize the neurons with low expression of α-synuclein, we performed immunostaining using a specific antibody against GAD, a well-known marker of inhibitory neurons. GAD-positive neurons were immunonegative for α-synuclein (Fig. 1A). Although GAD-positive puncta were juxtaposed with the α-synuclein-positive dendrites, most GAD signals were not colocalized with α-synuclein (Fig. 1A, merged images). 89±1.4% of GAD-positive neurons displayed no expression of α-synuclein (6 coverslips were analyzed). About 10% of the GAD-positive neurons, however, showed faint immunoreactivity for α-synuclein. Double immunofluorescence with antibodies against α-synuclein and parvalbumin or somatostatin, other marker proteins of inhibitory neurons, confirmed that α-synuclein was not detected in parvalbumin- or somatostatin-positive neurons (Fig. 1C and 1D). These results indicated that inhibitory neurons show very low expression of α-synuclein *in vitro*. Even after depletion of glial cells by AraC treatment, this differential expression pattern of α-synuclein was still observed (data not shown).

Cultured neurons exhibited differential expression of α-synuclein within 30 h after cell dissemination

To investigate the expression of α-synuclein during cell maturation, double immunostaining for NeuN, a neuron-specific marker, and α-synuclein was performed at various times after cell-disemination (Fig. 2A). Expression of α-synuclein gradually increased during cell maturation, and after 30 h cultured neurons already exhibited differential expression levels of α-synuclein. There were α-synuclein-negative neurons among the NeuN-positive cells. At this time point, GAD expression was not sufficient to distinguish inhibitory neurons (Fig. 2B).

α-Synuclein was localized at excitatory synapses

We examined the synaptic localization of α-synuclein by double immunostaining for α-synuclein and synaptotagmin, a presynaptic marker (Fig. 3A and 3B). Although α-synuclein was colocalized with synaptotagmin in some presynapses, a subset of the synaptotagmin-positive synapses lacked α-synuclein expression. In contrast, GAD immunoreactivity was colocalized with some of the signals of synapsin, another presynaptic marker (Fig. S1B). Because α-synuclein was not co-expressed with either GAD, parvalbumin, or somatostatin in nerve terminals (Fig. 1), α-synuclein-positive puncta are not likely to be presynapses of inhibitory neurons.

Further characterization by immunostaining for vGluT-1, an excitatory synaptic marker, revealed that almost all α-synuclein-positive synapses co-expressed vGluT-1 (Fig. 3C and 3D). We also confirmed that vGluT-1 was not colocalized with GAD (Fig. S1C). Furthermore, we performed quantitative colocalization analysis using Pearson's correlation test. The correlation of pixel intensities between α-synuclein and vGluT-1 was excellent (Fig. S2A; Pearson's correlation coefficient, $R = 0.83$). However, the correlations of pixel intensities between α-synuclein and inhibitory neuronal markers were weak (Fig. S2B, GAD $R = 0.20$;

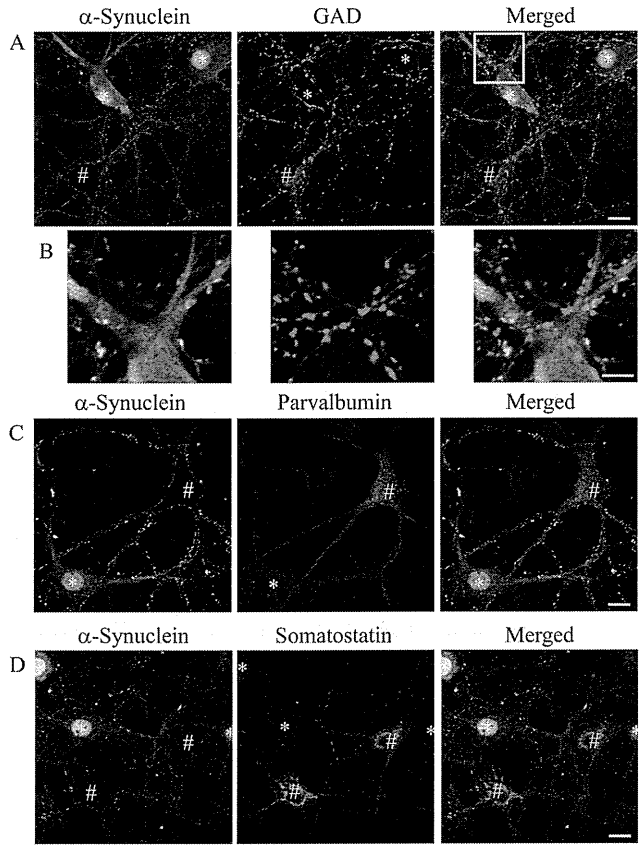

Figure 1. Low expression of α-synuclein in inhibitory neurons. Cells expressing the inhibitory neuronal marker proteins GAD (A), parvalbumin (C), and somatostatin (D) (indicated by #) showed low expression of α-synuclein. Cells with high expression of α-synuclein are labeled with asterisks. The region marked by a white square in A is magnified in B. Immunoreactivity of GAD was not colocalized with that of α-synuclein (B). Three independent cultures were performed and the differential expression pattern of α-synuclein was reproducibly confirmed. These images were further subjected to the quantitative colocalization analyses shown in Fig. S2. Scale bars: 10 μm in A, C, and D; 5 μm in B.
doi:10.1371/journal.pone.0089327.g001

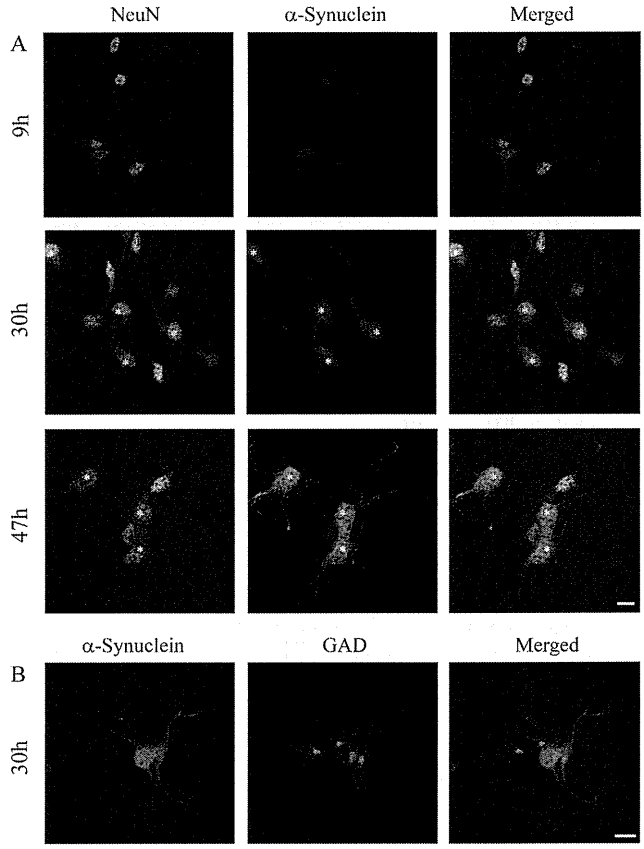

Figure 2. Differential expression of α-synuclein during cell maturation. (A) Expression of α-synuclein was examined at the indicated times after cell dissemination. Immunoreactivity of α-synuclein increased during cell maturation. By 30 h after cell dissemination, some NeuN-positive cells expressed α-synuclein (asterisks), but other NeuN-positive cells did not. (B) Expression of GAD at 30 h was not sufficient to distinguish inhibitory neurons from other types of neurons. Three independent cultures were performed. Scale bars: 10 μm.
doi:10.1371/journal.pone.0089327.g002

Fig. S2C, parvalbumin R = 0.38; Fig. S2D, somatostatin R = 0.14). These results indicated that *in vitro* α-synuclein was predominantly expressed in excitatory neurons, but not in inhibitory neurons.

α-Synuclein was colocalized with synapsin during presynaptic membrane recycling

Previous reports have demonstrated that α-synuclein is involved in SNARE-complex assembly and the resulting release of synaptic vesicles [12]. However, in this study some neurons were immunonegative for α-synuclein (Fig. 1). Depolarization by treatment with culture medium containing high potassium altered the synaptic localization of synapsin from synaptic vesicles to the presynaptic plasma membrane during exocytosis (Fig. 4). α-Synuclein was colocalized with synapsin during the presynaptic membrane recycling. This change in synapsin localization at synapses during depolarization also occurred in the absence of α-synuclein. This differential expression pattern was still evident at synapses following recovery from the membrane depolarization (Fig. 4). Activity-dependent recycling of synaptic membrane therefore seems to occur independently of the existence of α-synuclein.

GAD-positive neurons were free of intracellular aggregates of α-synuclein

Intracellular aggregates such as LBs and LNs are mainly composed of α-synuclein. These aggregates are formed by recruitment of intrinsic soluble α-synuclein into the insoluble aggregate core. Endogenous expression of α-synuclein, therefore, should be required for the formation of intracellular aggregates of α-synuclein [17]. Preformed fibrils prepared from recombinant α-synuclein can induce the formation of LB-like intracellular aggregates [17]. LB-like aggregates contain α-synuclein with a phosphorylated serine 129 residue [22]. If inhibitory neurons have low expression levels of α-synuclein, they may not be able to form intracellular aggregates, because of an inability to recruit endogenous α-synuclein. After treatment with preformed fibrils prepared from recombinant α-synuclein (Fig. S3), intracellular fibrous aggregates or inclusion bodies were detected by a specific antibody against phosphorylated α-synuclein (Fig.5A and 5B). This antibody can exclusively detect intracellular aggregates of α-synuclein [22]. As expected, most GAD-positive neurons were free of intracellular aggregates of α-synuclein (Fig. 5A). We also performed quantitative colocalization analysis using Pearson's correlation test. The correlation of pixel intensities between phosphorylated α-synuclein and GAD was weak (Fig. S2E;

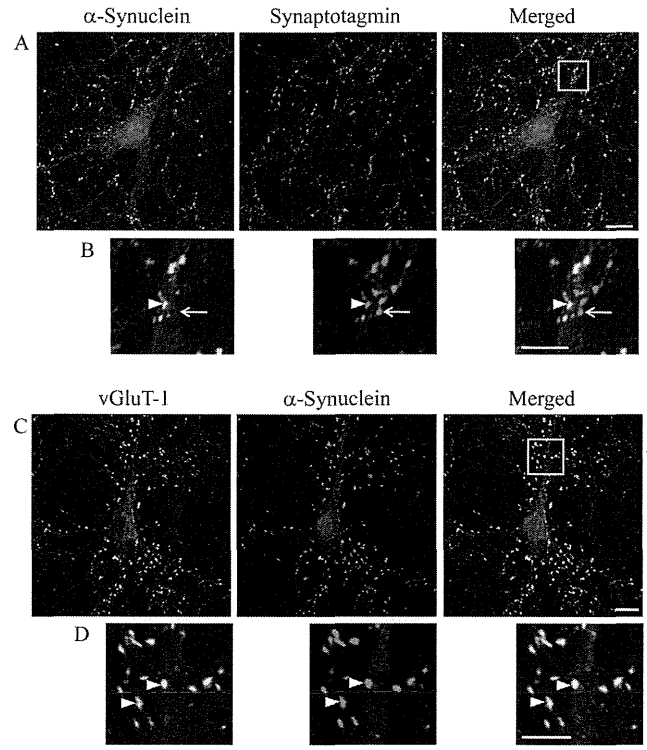

Figure 3. Presynaptic localization of α-synuclein in excitatory neurons. (A, B) Confocal images of double immunostaining for α-synuclein and synaptotagmin. The region marked by a white square in A is magnified in B. Arrowhead in B indicates the presynapse, expressing both α-synuclein and synaptotagmin. However, there are some synaptotagmin-positive synapses lacking α-synuclein (arrow). (C, D) Confocal images of double immunostaining for α-synuclein and vGluT-1, an excitatory neuronal marker protein. The region marked by a white square in C is magnified in D. α-Synuclein is colocalized with vGluT-1 in D (arrowheads). Three independent cultures were performed and colocalization between α-synuclein and vGluT-1 was reproducibly confirmed. Panel C was subjected to the quantitative colocalization analysis shown in Fig. S2. Scale bars: 10 μm in A and C; 5 μm in B and D.
doi:10.1371/journal.pone.0089327.g003

R = 0.07). The proportion of aggregate-containing GAD-positive cells was significantly lower than that of NeuN-positive cells (see note "a" in Table 1). This result is probably due to the lower amount of endogenous α-synuclein expressed in the GAD-positive cells. Another possibility is that the cell entry efficiency of the seeds derived from the preformed fibrils was different between inhibitory neurons and other types of neurons. Next, we confirmed the dose-dependent effect of the intracellular amount of α-synuclein on aggregate formation. After transfection of human α-synuclein and further treatment with preformed fibrils, intracellular accumulation of exogenous α-synuclein was observed in GAD-positive neurons. We used the Syn211 monoclonal antibody to detect only exogenous expression of human α-synuclein without detecting endogenous mouse α-synuclein, and prepared preformed fibrils from mouse α-synuclein. Before fibril treatment, exogenous human α-synuclein was diffusely expressed in the cell body (Fig. 5C). After fibril treatment, accumulation of exogenous α-synuclein was observed in some of the transfected GAD-positive cells (Fig. 5C and Table 1). The efficiency of aggregate formation was significantly increased by exogenous expression of α-synuclein (see note "b" in Table 1). These results indicated that inhibitory neurons can form intracellular aggregates under conditions where there is sufficient intracellular α-synuclein.

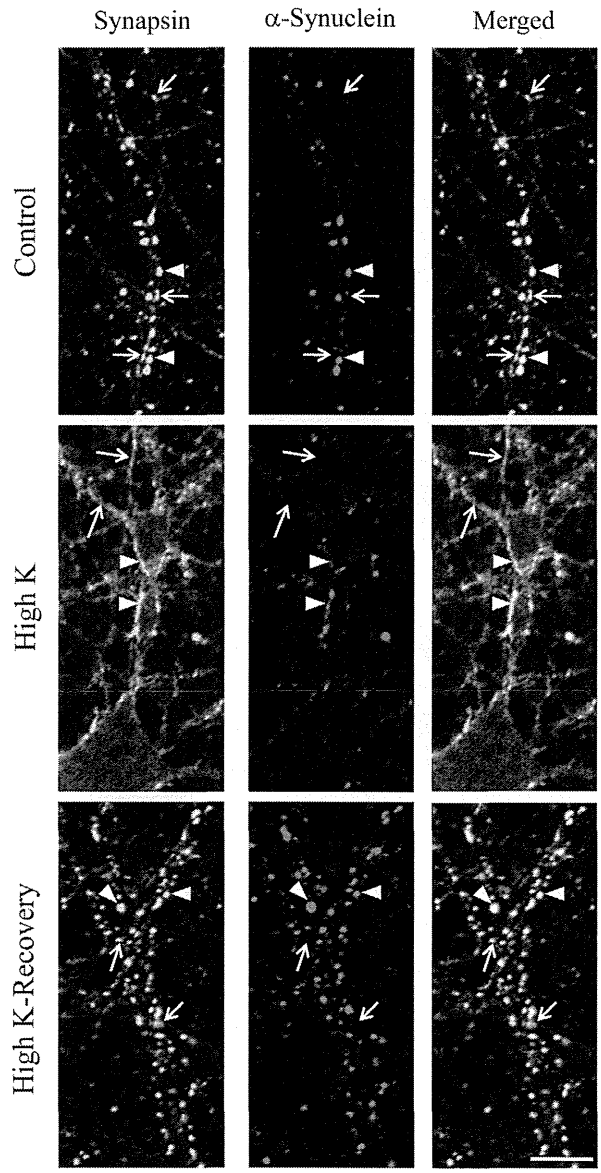

Figure 4. Colocalization of synapsin and α-synuclein during presynaptic membrane recycling. Synapsin immunoreactivity was observed as punctate signals before treatment (Control). After membrane depolarization by applying a medium containing high potassium, the punctate signals of synapsin changed shape and fused to the presynaptic plasma membrane (High K). The change in localization was reversed by treatment with a low-potassium medium (High K-Recovery). α-Synuclein was colocalized with synapsin during presynaptic membrane recycling (arrowheads). However, there are also instances of synapsin immunoreactivity without α-synuclein expression (arrows). Three independent cultures were performed, and these staining patterns were observed in all cultures. Scale bar: 5 μm.
doi:10.1371/journal.pone.0089327.g004

Low expression of α-synuclein in GAD-positive cells was also conserved *in vivo*

In sections of mouse hippocampus, α-synuclein was detected as puncta in the periphery of neurons. Diffuse expression of α-synuclein was not observed in the cell body or nucleus. α-Synuclein was colocalized with vGluT-1 in the CA1 region (Fig. 6A and 6B). In contrast, α-synuclein was juxtaposed with the punctuate immunoreactivity of GAD and never colocalized with GAD signals (Fig. 6C and 6D). Furthermore, acquired confocal

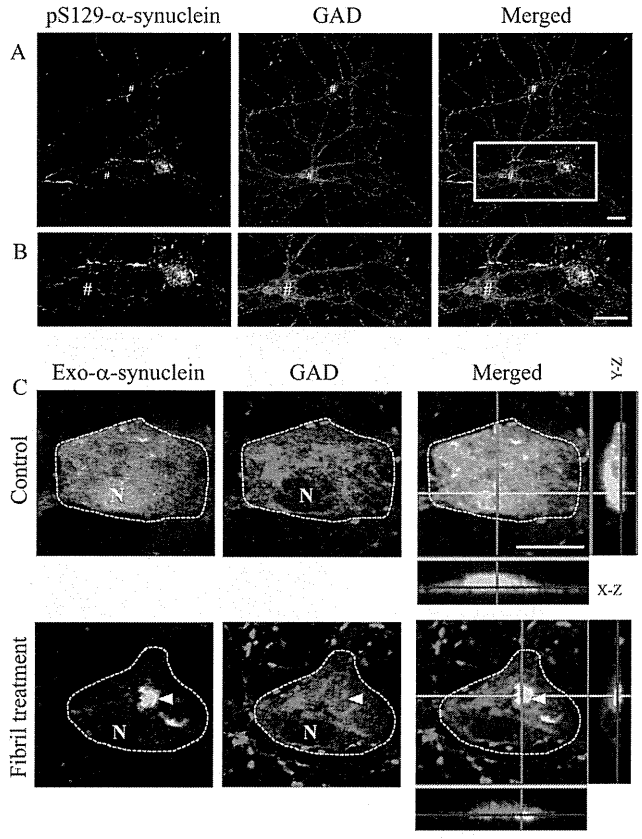

Figure 5. Formation of intracellular aggregates of α-synuclein. (A) Confocal images of double immunostaining for phosphorylated α-synuclein and GAD after treatment with preformed fibrils of α-synuclein. The region marked by a white square in A is magnified in B. Immunoreactivity of phosphorylated α-synuclein was observed as intracellular fibrous aggregates or inclusion bodies. GAD-positive neurons indicated by # were free of α-synuclein aggregate formation. GAD signals, including GAD-positive neurites, were not colocalized with phosphorylated α-synuclein. (C) In the absence of fibril treatment, exogenous human α-synuclein was diffusely distributed in the cell body of GAD neurons (Control). After fibril treatment, intracellular inclusions positive for α-synuclein were induced in the GAD-positive cells expressing exogenous α-synuclein. Cell bodies are shown surrounded by white dotted lines. 'N' indicates the location of the nucleus. Three independent cultures were performed and in all cases confirmed that intracellular inclusions were predominantly formed in GAD-negative neurons. Exogenous expression of human α-synuclein enhanced the aggregate formation in GAD-positive cells. These results were quantified and are described in Table 1. Scale bars: 10 μm.
doi:10.1371/journal.pone.0089327.g005

images were subjected to the quantitative colocalization analysis. The correlation of pixel intensities between the α-synuclein and vGluT-1 shown in Fig. 6A was excellent (Fig. S2F; $R = 0.78$). In contrast, the correlation of α-synuclein and GAD was weak (Fig. S2G; $R = 0.11$). Thus the expression pattern of α-synuclein observed in cultured inhibitory neurons was also conserved *in vivo*.

Discussion

α-Synuclein is localized at presynapses [7,8] and it was shown to regulate the size of the presynaptic vesicular pool in a study where antisense oligonucleotides were introduced in cultured hippocampal neurons [23]. More recently, using knockout and overexpressing neurons, Scott and Roy showed that α-synuclein plays a role in maintaining the overall size of the recycling pool of vesicles [13].

Table 1.

Ratio	%
pS129-α-Synuclein-positive cells/NeuN-positive cells	35±0.89[a]
pS129-α-Synuclein-positive cells/GAD-positive cells	2.7±0.64[a*]
Aggregate-positive cells/GAD- and syn211-positive cells	24±2.2[b*]

[a]Data represent mean ± SEM (6 coverslips). Two independent cultures were performed and three coverslips per culture were used for the immunocytochemical study. Statistical analysis showed significant difference with $p<0.0001$ by student's t test unpaired, two-tailed.
[b]Data represent mean ± SEM (4 coverslips). Two independent cultures were performed and two coverslips per culture were used for the immunocytochemical study. Asterisk indicates significant difference with $p<0.01$ by student's t test unpaired, two-tailed with Welch's correction.
doi:10.1371/journal.pone.0089327.t001

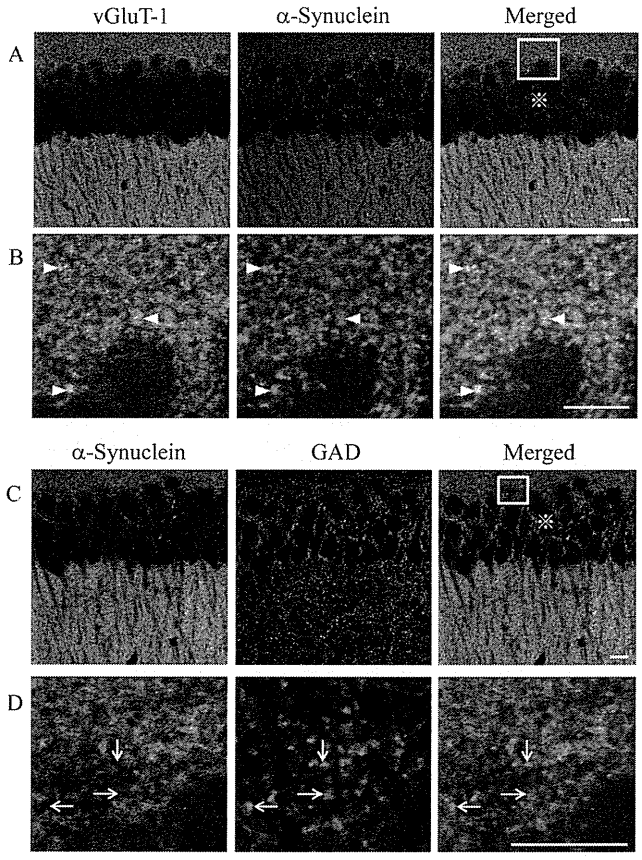

Figure 6. Localization of α-synuclein in the hippocampal CA1 region. (A, B) Confocal images of hippocampal neurons double immunostained for vGluT-1 and α-synuclein. The region marked by a white square in A is magnified in B. α-Synuclein is colocalized with vGluT-1 in B (arrowheads). (C, D) Confocal images double immunostained for α-synuclein and GAD. The region marked by a white square in C is magnified in D. As indicated by arrows in D, colocalization of α-synuclein and GAD was not detected. Mouse brains from two littermates were used for the immunohistochemical study. This experiment was repeated three times, and the differential expression pattern of α-synuclein was reproducibly confirmed. Panels A and C were used for the quantitative colocalization analyses shown in Fig. S2. Scale bars: 10 μm. ※ indicates stratum pyramidale.
doi:10.1371/journal.pone.0089327.g006

We observed expression and synaptic localization of α-synuclein in excitatory neurons, but not in inhibitory neurons, although there were no obvious differences between the two types of neurons in expression of the synaptic markers synaptotagmin and synapsin. We also observed that activity-dependent presynaptic membrane recycling (induced by high potassium treatment) occurred independently of the presence of α-synuclein.

While there have been many studies investigating the properties of postsynaptic channels including kinetics [24–26] and the signaling molecules involved in synaptic transduction [27], less is known about the presynaptic differences between excitatory and inhibitory neurons. Recent work revealed that the sizes of both the recycling pool and total vesicular pool are more variable at glutamatergic synapses than gamma-aminobutyric acid (GABAergic) synapses [28]. This heterogeneity of the size of the recycling pool at glutamatergic synapses may provide a dynamic range of synaptic strength that is not present at GABAergic synapses [28,29]. α-Synuclein might act as a modulator of the size of the recycling pool at excitatory synapses. α-Synuclein is also suggested to be involved in mobilization of glutamate from the reserve pool using electrophysiology of hippocampal slices [30].

There is a possibility that the differential expression of α-synuclein is due to a difference in protein turnover between excitatory and inhibitory neurons. However, treatment with inhibitors of proteasomes or lysosomes did not alter the immunostaining patterns of α-synuclein (data not shown), suggesting that differential synthesis rather than degradation of α-synuclein is responsible for the distinct expression patterns in neurons.

Recently, it was reported that α-synuclein promotes early neurite outgrowth in cultured primary neurons [31]. It has also been suggested that α-synuclein plays important roles in the early development of synapses [10]. The expression ratio of α-synuclein/synaptophysin is higher during early development than in adult and aged rat brain [11]. We demonstrated that cultured neurons exhibit differential expression of α-synuclein by 30 h after cell dissemination. At this stage, there were no synaptic connections established between neurons. In addition, expression of GAD was very weak and not strong enough to distinguish inhibitory neurons. These results suggest that α-synuclein is involved in the differentiation of neurons.

Concerning the pathogenicity of α-synuclein, we observed that inhibitory neurons did not exhibit aggregate formation after treatment with preformed fibrils. This result was due to the low expression level of α-synuclein, because the expression of exogenous human α-synuclein in GAD neurons enabled them to form α-synuclein aggregates. A study in DLB patients showed that parvalbumin-containing cortical neurons are free of LBs and spared from degeneration, although the basal expression level of α-synuclein in these neurons was not determined [16]. In addition, it was found that overexpression of α-synuclein in a transgenic mice model caused inclusion body formation in hippocampal neurons, suggesting that high expression of α-synuclein is important for the intracellular accumulation and formation of LBs [14]. Recently, accumulation of α-synuclein was observed at the presynaptic terminals expressing vGluT-1in SNARE protein (SNAP-25) mutant mice [32].

These reports seem to be consistent with our present results. Intracellular aggregate formation composed of α-synuclein might be related to the endogenous expression level of α-synuclein, which is cell-type specific.

In conclusion, we have demonstrated differential expression patterns of α-synuclein between excitatory and inhibitory neurons *in vitro*. Importantly, these observations were also confirmed *in vivo*. Further studies will elucidate how α-synuclein works differently in the synaptic machinery of excitatory and inhibitory neurons, including in the regulation of the membrane recycling pool. Further analysis of the regulation of intracellular expression of α-synuclein will provide new insights for understanding the pathological conditions of neurodegenerative disorders including PD and DLB.

Supporting Information

Figure S1 Double staining for NeuN and α-synuclein. (A) Confocal images of cultured hippocampal neurons double immunostained for NeuN and α-synuclein. α-Synuclein was differentially expressed among the NeuN-positive cells. (B) GAD-immunoreactive puncta occupied a part of the synapsin-positive synapses. (C) Immunoreactivity of GAD was not colocalized with that of vGluT-1. Two independent cultures were performed and the reactivity of the antibodies was confirmed. Scale bars: 10 μm in A; 5 μm in B and C.
(TIF)

Figure S2 Quantification of colocalization between α-synuclein and marker proteins. (A–G) The degree of the colocalization shown in Figs. 3C, 1A, 1C, 1D, 5A, 6A, and 6C was determined using LSM colocalization analysis and quantified using Pearson's correlation coefficient (R).
(TIF)

Figure S3 Preparation of fibrils of α-synuclein. (A) Purity of the recombinant α-synuclein was confirmed by SDS-PAGE. Lane M indicates the molecular masses, given in kilodaltons. His-tagged α-synuclein was detected as a 20 kDa band (lane F). This fraction predominantly contained the induced protein. CBB: Coomassie Brilliant Blue staining. (B) Western blot analysis of α-synuclein. α-Synuclein was oligomerized by agitation and the insoluble aggregates with high molecular masses were recovered in the precipitant after ultracentrifugation (Lane P). Lane Or: original fraction before agitation; Lane S: supernatant after ultracentrifugation; IB: immunoblot.
(TIF)

Acknowledgments

The hybridoma-producing monoclonal anti-synaptotagmin antibody developed by Dr. Louis Reichardt was obtained from the Developmental Studies Hybridoma Bank developed under the auspices of the NICHD and maintained by The University of Iowa, Department of Biology, Iowa City, IA, USA.

Author Contributions

Conceived and designed the experiments: KT MT. Performed the experiments: KT YW AT HT. Analyzed the data: KT YW TT MT MT. Contributed reagents/materials/analysis tools: AT HT SM. Wrote the paper: KT MT.

References

1. Stefanis L (2012) alpha-Synuclein in Parkinson's disease. Cold Spring Harb Perspect Med 2: a009399.
2. Dickson DW (2001) Alpha-synuclein and the Lewy body disorders. Curr Opin Neurol 14: 423–432.

3. Spillantini MG, Crowther RA, Jakes R, Hasegawa M, Goedert M (1998) alpha-Synuclein in filamentous inclusions of Lewy bodies from Parkinson's disease and dementia with lewy bodies. Proc Natl Acad Sci U S A 95: 6469–6473.
4. Polymeropoulos MH, Lavedan C, Leroy E, Ide SE, Dehejia A, et al. (1997) Mutation in the alpha-synuclein gene identified in families with Parkinson's disease. Science 276: 2045–2047.
5. Zarranz JJ, Alegre J, Gomez-Esteban JC, Lezcano E, Ros R, et al. (2004) The new mutation, E46K, of alpha-synuclein causes Parkinson and Lewy body dementia. Ann Neurol 55: 164–173.
6. Kruger R, Kuhn W, Muller T, Woitalla D, Graeber M, et al. (1998) Ala30Pro mutation in the gene encoding alpha-synuclein in Parkinson's disease. Nat Genet 18: 106–108.
7. Vivacqua G, Casini A, Vaccaro R, Fornai F, Yu S, et al. (2011) Different subcellular localization of alpha-synuclein in the C57BL/6J mouse's central nervous system by two novel monoclonal antibodies. J Chem Neuroanat 41: 97–110.
8. Withers GS, George JM, Banker GA, Clayton DF (1997) Delayed localization of synelfin (synuclein, NACP) to presynaptic terminals in cultured rat hippocampal neurons. Brain Res Dev Brain Res 99: 87–94.
9. Totterdell S, Meredith GE (2005) Localization of alpha-synuclein to identified fibers and synapses in the normal mouse brain. Neuroscience 135: 907–913.
10. Hsu LJ, Mallory M, Xia Y, Veinbergs I, Hashimoto M, et al. (1998) Expression pattern of synucleins (non-Abeta component of Alzheimer's disease amyloid precursor protein/alpha-synuclein) during murine brain development. J Neurochem 71: 338–344.
11. Petersen K, Olesen OF, Mikkelsen JD (1999) Developmental expression of alpha-synuclein in rat hippocampus and cerebral cortex. Neuroscience 91: 651–659.
12. Burre J, Sharma M, Tsetsenis T, Buchman V, Etherton MR, et al. (2010) Alpha-synuclein promotes SNARE-complex assembly in vivo and in vitro. Science 329: 1663–1667.
13. Scott D, Roy S (2012) alpha-Synuclein inhibits intersynaptic vesicle mobility and maintains recycling-pool homeostasis. J Neurosci 32: 10129–10135.
14. Masliah E, Rockenstein E, Veinbergs I, Mallory M, Hashimoto M, et al. (2000) Dopaminergic loss and inclusion body formation in alpha-synuclein mice: implications for neurodegenerative disorders. Science 287: 1265–1269.
15. Winner B, Regensburger M, Schreglmann S, Boyer L, Prots I, et al. (2012) Role of alpha-synuclein in adult neurogenesis and neuronal maturation in the dentate gyrus. J Neurosci 32: 16906–16916.
16. Gomez-Tortosa E, Sanders JL, Newell K, Hyman BT (2001) Cortical neurons expressing calcium binding proteins are spared in dementia with Lewy bodies. Acta Neuropathol 101: 36–42.
17. Volpicelli-Daley LA, Luk KC, Patel TP, Tanik SA, Riddle DM, et al. (2011) Exogenous alpha-synuclein fibrils induce Lewy body pathology leading to synaptic dysfunction and neuron death. Neuron 72: 57–71.
18. Giasson BI, Jakes R, Goedert M, Duda JE, Leight S, et al. (2000) A panel of epitope-specific antibodies detects protein domains distributed throughout human alpha-synuclein in Lewy bodies of Parkinson's disease. J Neurosci Res 59: 528–533.
19. Morita S, Miyata S (2012) Synaptic localization of growth-associated protein 43 in cultured hippocampal neurons during synaptogenesis. Cell Biochem Funct.
20. Watanabe Y, Tatebe H, Taguchi K, Endo Y, Tokuda T, et al. (2012) p62/SQSTM1-dependent autophagy of Lewy body-like alpha-synuclein inclusions. PLoS One 7: e52868.
21. Tatebe H, Watanabe Y, Kasai T, Mizuno T, Nakagawa M, et al. (2010) Extracellular neurosin degrades alpha-synuclein in cultured cells. Neurosci Res 67: 341–346.
22. Fujiwara H, Hasegawa M, Dohmae N, Kawashima A, Masliah E, et al. (2002) alpha-Synuclein is phosphorylated in synucleinopathy lesions. Nat Cell Biol 4: 160–164.
23. Murphy DD, Rueter SM, Trojanowski JQ, Lee VM (2000) Synucleins are developmentally expressed, and alpha-synuclein regulates the size of the presynaptic vesicular pool in primary hippocampal neurons. J Neurosci 20: 3214–3220.
24. Shah MM, Hammond RS, Hoffman DA (2010) Dendritic ion channel trafficking and plasticity. Trends Neurosci 33: 307–316.
25. Greger IH, Ziff EB, Penn AC (2007) Molecular determinants of AMPA receptor subunit assembly. Trends Neurosci 30: 407–416.
26. Luscher B, Keller CA (2004) Regulation of GABAA receptor trafficking, channel activity, and functional plasticity of inhibitory synapses. Pharmacol Ther 102: 195–221.
27. Sheng M, Kim E (2011) The postsynaptic organization of synapses. Cold Spring Harb Perspect Biol 3.
28. Moulder KL, Jiang X, Taylor AA, Shin W, Gillis KD, et al. (2007) Vesicle pool heterogeneity at hippocampal glutamate and GABA synapses. J Neurosci 27: 9846–9854.
29. Moulder KL, Mennerick S (2005) Reluctant vesicles contribute to the total readily releasable pool in glutamatergic hippocampal neurons. J Neurosci 25: 3842–3850.
30. Gureviciene I, Gurevicius K, Tanila H (2007) Role of alpha-synuclein in synaptic glutamate release. Neurobiol Dis 28: 83–89.
31. Liu G, Wang P, Li X, Li Y, Xu S, et al. (2013) Alpha-synuclein promotes early neurite outgrowth in cultured primary neurons. J Neural Transm.
32. Nakata Y, Yasuda T, Fukaya M, Yamamori S, Itakura M, et al. (2012) Accumulation of alpha-synuclein triggered by presynaptic dysfunction. J Neurosci 32: 17186–17196.

EXPERIMENTAL CELL RESEARCH 326 (2014) 36–45

Available online at www.sciencedirect.com

ScienceDirect

journal homepage: www.elsevier.com/locate/yexcr

Research Article

Genetic link between Cabeza, a Drosophila homologue of Fused in Sarcoma (FUS), and the EGFR signaling pathway

Mai Shimamura[a,b,1], *Akane Kyotani*[a,b], *Yumiko Azuma*[c], *Hideki Yoshida*[a,b], *Thanh Binh Nguyen*[a,b], *Ikuko Mizuta*[c], *Tomokatsu Yoshida*[c], *Toshiki Mizuno*[c], *Masanori Nakagawa*[d], *Takahiko Tokuda*[c,e,**], *Masamitsu Yamaguchi*[a,b,*]

[a]*Department of Applied Biology, Kyoto Institute of Technology, Matsugasaki, Sakyo-ku, Kyoto 606-8585, Japan*
[b]*Insect Biomedical Research Center, Kyoto Institute of Technology, Matsugasaki, Sakyo-ku, Kyoto 606-8585, Japan*
[c]*Department of Neurology, Kyoto Prefectural University of Medicine, 465 Kajii-cho,Kamigyo-ku, Kyoto 602-8566, Japan*
[d]*North Medical Center, Kyoto Prefectural University of Medicine, 465 Kajii-cho, Kamigyo-ku, Kyoto 602-8566, Japan*
[e]*Department of Molecular Pathobiology of Brain Diseases, Graduate School of Medical Science, Kyoto Prefectural University of Medicine, 465 Kajii-cho, Kamigyo-ku, Kyoto 602-8566, Japan*

ARTICLE INFORMATION

Article Chronology:
Received 10 January 2014
Received in revised form
17 May 2014
Accepted 4 June 2014
Available online 11 June 2014

Keywords:
Amyotrophic lateral sclerosis
Cabeza
Retina
EGFR pathway
Drosophila

ABSTRACT

Amyotrophic Lateral Sclerosis (ALS) is a fatal neurodegenerative disease that causes progressive muscular weakness. Fused in Sarcoma (*FUS*) that has been identified in familial ALS is an RNA binding protein that is normally localized in the nucleus. However, its function in vivo is not fully understood. *Drosophila* has Cabeza (Caz) as a *FUS* homologue and specific knockdown of Caz in the eye imaginal disc and pupal retina using a *GMR-GAL4* driver was here found to induce an abnormal morphology of the adult compound eyes, a rough eye phenotype. This was partially suppressed by expression of the apoptosis inhibitor P35. Knockdown of Caz exerted no apparent effect on differentiation of photoreceptor cells. However, immunostaining with an antibody to Cut that marks cone cells revealed fusion of these and ommatidia of pupal retinae. These results indicate that Caz knockdown induces apoptosis and also inhibits differentiation of cone cells, resulting in abnormal eye morphology in adults. Mutation in EGFR pathway-related genes, such as *rhomboid-1*, *rhomboid-3* and mirror suppressed the rough eye phenotype induced by Caz

Abbreviations: Caz, Cabeza; ALS, Amyotrophic Lateral Sclerosis; *FUS*, Fused in Sarcoma; EGFR, Epidermal growth factor-receptor; SOD1, Cu/Zn superoxide dismutase; TDP-43, TAR DNA-binding protein of 43 kDa gene; CNS, central nervous system; APF, after pupal formation; ERK, Extracellular signal-related kinase.

*Corresponding author at: Department of Applied Biology, Kyoto Institute of Technology, Matsugasaki, Sakyo-ku, Kyoto 606–8585, Japan. Fax: +81 75 724 7799.

**Corresponding author at: Department of Molecular Pathobiology of Brain Diseases (Neurology), Graduate School of Medical Science, Kyoto Prefectural University of Medicine, 465 Kajii-cho, Kamigyo-ku, Kyoto 602–8566, Japan. Fax: +81 75 211 8645.

E-mail addresses: ttokuda@koto.kpu-m.ac.jp (T. Tokuda), myamaguc@kit.ac.jp (M. Yamaguchi).

[1] Present address: Environmental Research Laboratory of Public Health, Kankyo Eisei Yakuhin Co. Ltd., 3-6-2, Hikaridai, Seika-cho, Soraku-gun, Kyoto, Kyoto 619-0237, Japan

http://dx.doi.org/10.1016/j.yexcr.2014.06.004

knockdown. Moreover, the *rhomboid-1* mutation rescued the fusion of cone cells and ommatidia observed in Caz knockdown flies. The results suggest that Caz negatively regulates the EGFR signaling pathway required for determination of cone cell fate in *Drosophila*.

Introduction

Amyotrophic lateral sclerosis (ALS) is a fatal neurodegenerative disease that is characterized by degeneration of upper and lower motor neurons of the brain and the spinal cord, which leads to progressive muscle weakness and fatal paralysis [1]. Most cases of ALS are sporadic, but some patients have a familial history as a result of a mutation in the gene for Cu/Zn superoxide dismutase (SOD1) [2].

The family of MAPKs includes ERK, p38 and JNK. Each MAPK signaling pathway consists of at least three components, a MAPK kinase kinase, a MAPK kinase and a MAPK. Deviation from strict control of MAPK signaling pathways has been implicated in the development of human neurodegenerative diseases including Alzheimer's, Parkinson's and ALS [3]. Recently it was reported that aberrant expression and activation of p38 in motor neurons and microglia play important roles in ALS progression [4]. Persistent activation of p38 correlates with degeneration of motor neurons in transgenic mice expressing a mutant SOD1 [5,6]. Moreover a p38 inhibitor was demonstrated to prevent the apoptosis of motor neurons induced by a mutant SOD1 [7]. Thus a possible link between MAPK signaling and ALS has been suggested.

A substantial number of proteins linked to ALS are directly or indirectly involved in RNA processing [8]. Among RNA-binding proteins, mutations in the TAR DNA-binding protein of 43 kDa gene (*TDP-43*) and fused in sarcoma (*FUS*) gene have been identified as major genetic causes in both familial and sporadic ALS [9–18]. *TDP-43* and *FUS* are implicated in multiple aspects of RNA metabolism including transcriptional regulation, mRNA splicing and mRNA shuttling between the nucleus and the cytoplasm [19,20].

Drosophila has a single orthologue of human *FUS*, named Cabeza (*Caz*). In situ hybridization and immunohistochemistrical analyses demonstrated that *Caz* mRNA and protein are enriched in the brain and central nervous system (CNS) during embryogenesis, and the *Caz* protein has been detected in the nuclei of several larval tissues and in imaginal discs [21,22]. The full-length recombinant *Caz* protein and its RRM domain are capable of binding RNA in vitro [21]. These findings suggest that *Caz* is a nuclear RNA binding protein that may play an important role in the regulation of RNA metabolism during *Drosophila* development.

In our previous studies using neuron specific *Caz* knockdown flies, we demonstrated that *Caz* functions in neuronal cell bodies and/or axons of the CNS and is involved in elongation of synaptic branches of motoneurons [22]. However, contributions of *Caz* during development of various tissues in *Drosophila* are not fully understood. As a first step toward clarification, we investigated the effect of knockdown of *Caz* on eye development and revealed a rough eye phenotype, accompanied by apoptosis, abnormal differentiation of cone cells and defects in ommatidia rotation. In addition, a *Rhomboid-1* mutant could be shown to rescue the fusion of cone cells and mutations of *rhomboid-3* and *mirror* significantly suppressed the rough eye phenotype of the *Caz* knockdown flies. Since *rhomboid-1*, *rhomboid-3*, and *mirror* are EGFR pathway-related genes, these results indicate genetic links between *Caz* and EGFR signaling.

Materials and methods

Fly stocks

Fly stocks were maintained at 25 °C on standard food containing 0.7% agar, 5% glucose and 7% dry yeast. Canton S was used as the wild type. *w*; *UAS-Caz-IR*$_{363-399}$;+(CG3606) and *UAS-rho-IR*^{28690} was obtained from Vienna *Drosophila* RNAi Center (VDRC). The RNAi of this strain was targeted to the region corresponding to residues 363–399 of *Drosophila Caz* (*UAS-Caz-IR*$_{363-399}$). Four and seven transgenic strains carrying *UAS-Caz-IR*$_{1-167}$ and *UAS-Caz-IR*$_{180-346}$ were established [22]. Each transgenic strain showed a consistent phenotype. Alleles of the following genes were obtained from the Bloomington *Drosophila* stock center: *mirror*^{SaiD3}, *ru*^{1}, *rho*^{7M43} and *rho*^{AA69}. Enhancer trap lines carrying the lacZ markers AE127 (inserted into *seven-up*) [23] and *P82* (inserted into *deadpan*) [24] were obtained from Y. Hiromi and co- workers. These lines express the β-galactosidase marker in photoreceptor cells (R) of R3/R4/R1/R6 and R3/R4/R7. *hspFlp; +; tub*1> *FRT cd2 FRT> GAL4, UAS-GFP/ TM3* was a kind gift from A. Plessis. Establishment of lines carrying GMR-GAL4 was as described earlier [25]. Act5C-GAL4/ TM6B was also obtained from the Bloomington *Drosophila* stock center.

Generation of RNAi clones in retinae

RNAi clones in retinae were generated with the flip-out system [26]. Female flies with *hspFlp; +; tub*1> *FRT cd2 FRT> GAL4, UAS-GFP/ TM3* were crossed with *w; UAS-Caz-IR*$_{363-399}$;+male flies and clones were marked by the presence of GFP. Flip-out was induced 24–48 h after egg laying with a 60 min heat shock at 37 °C.

Immunostaining

For immunohistochemistory, larval eye imaginal discs and pupal retinae were dissected, and fixed in 4% paraformaldehyde/ PBS for 15 min and 30 min at 25 °C, respectively. After washing with PBS containing 0.3% Triton X-100, the samples were blocked with PBS containing 0.15% Triton X-100 and 10% normal goat serum for 30 min at 25 °C, and incubated with diluted primary antibodies in PBS containing 0.15% Triton X-100 and 10% normal goat serum for 16 h at 4 °C. The following antibodies were used; mouse anti-LacZ (1:500, Developmental Studies Hybridoma Bank [DSHB], 40-1a), mouse anti-Elav (1:200 DSHB 9F8A9), mouse anti-Cut (1:500, DSHB 2B10), mouse anti-Discs large (1:500) (DSHB) and anti-diphospho ERK (dpERK) (1: 500) (Sigma). After extensive washing

with PBS containing 0.3% Triton X-100, samples were incubated with secondary antibodies labeled with either Alexa 546 or Alexa 488 (1:400, Invitrogen) for 3 h at 25 °C. Alexa 488-conjugated phalloidin (200 units/ ml) was used for the detection of F-actin. After extensive washing with PBS containing 0.3% Triton X-100, samples were mounted in Vectashield (Vector Laboratories Inc.) and analyzed by confocal laser scanning microscopy (Olympus Flouview FV10i).

Western immunoblot analysis

Protein extracts from the whole pupae of *Drosophila* carrying *Act5C-GAL4/+* or *Act5C-GAL4/+*; *UAS-Caz-IR*$_{363-399}$/+ were prepared as previously described [22]. The homogenates were boiled at 100 °C for 5 min, and then centrifuged. The supernatants (extracts) were electrophoretically separated on SDS-polyacrylamide gels containing 12% acrylamide and then transferred to polyvinylidene difluoride (PVDF) membranes (Bio-Rad). The blotted membranes were blocked with TBS/0.05% Tween containing 5% skim milk for 1 h at 25 °C, followed by incubation with rabbit polyclonal anti-*Caz* at a 1:5,000 dilution for 16 h at 4 °C. After washing, the membranes were incubated with HRP-conjugated anti-rabbit IgG (GE Healthcare Bioscience) at 1:10,000 dilution for 2 h at 25 °C. Antibody binding was detected using ECL Western blotting detection reagents (GE Healthcare Bioscience) and images were analyzed using a Lumivision Pro HSII image analyzer (Aisin Seiki).

Apoptosis assay

Third instar larvae or 42APF pupae were dissected in PBS and the eye imaginal discs or pupal retinae were fixed in 4% paraformaldehyde in PBS for 30 min at 25 °C. After being washed with 0.3% PBST, the sample were permeabilized by incubation in 0.25% PBST for 20 min in 25 °C. After washing with H_2O, the TUNEL reaction was carried out using a Click-iT TUNEL Alexa Fluor 594 Imaging Assay Kit (Life Technologies) according to the manufacture's recommendations.

Scanning electron microscopy

Adult flies were anesthetized, mounted on stages, and observed under a scanning electron microscope (SEM) VE-7800 (Keyence Inc.) in the low vacuum mode. The eye phenotype of at least five adult male flies (3 to 5 days old) of each line was examined in each experiment and the experiments were done in triplicate. No significant variation in eye phenotype was observed among the five individuals.

Data analysis

Quantification of intensity of *Caz* signals was carried out with six to nine different samples by using Meta Morph software (Molecular Devices). For the statistical analysis, Microsoft Excel 2007 was used. *P*-values were calculated using Welch's *t*-test and the error bars represent Standard Errors from Means.

Results

Knockdown of *Caz* in eye imaginal discs induces morphologically aberrant rough eyes

In order to investigate in vivo functions of *Caz*, we examined the effect of reduction of *Caz* protein in vivo using a combination of the GAL4-UAS targeted expression system and the RNAi method. Knockdown of *Caz* in all tissues by the Act5C-GAL4 driver strain resulted in late pupal lethality in transgenic lines carrying *UAS-Caz-IR*$_{1-167}$ (data not shown). Knockdown of *Caz* in eye imaginal discs by the GMR-GAL4 driver strain, in which *Caz* double-stranded RNA (dsRNA) was expressed in the region posterior to the morphogenetic furrow, induced morphologically aberrant rough eyes. SEM images showed fusion of ommatidia and a lack of bristles (Fig. S1C–F). Flies carrying GMR-GAL4 alone exhibited apparently normal eye morphology (Fig. S1A, and B). Moreover, to eliminate the possibility of off-target effects, we established eleven independent transgenic fly lines carrying *UAS-Caz-IR* targeted to the different regions of the *Caz* mRNA assessed in a previous study [22]. Phenotypes of the established transgenic fly lines crossed with the GMR-GAL4 driver strain are reported [27]. Each independent strain showed the similar rough eye phenotype as the flies carrying *UAS-Caz-IR* targeted to different regions of the *Caz* mRNA (Fig. S1C–F). These results suggest that the rough eye phonotype observed in *Caz* knockdown flies is not due to a possible insertional mutation or off-target effect but rather to reduction of the *Caz* protein level. Throughout the following studies, we utilized the strain CG3606 carrying *UAS-Caz-IR*$_{363-399}$.

To investigate whether the expression of *Caz* dsRNA efficiently reduces the level of *Caz* protein, we performed immunostaining of pupal retinae for 42 h after pupal formation (APF) with anti-*Caz* antibodies. We utilized the flip-out system to produce the RNAi clone so that the level of *Caz* could be directly compared within a single retina. We used *UAS-Caz-IR*$_{363-399}$ line, since it apparently showed the severest rough eye (Fig. S1E and F). Within the RNAi clone of *Caz* marked by the presence of GFP signals, *Caz* signals marked by Red were reduced by 50% (Fig. 1A to G). Double immunostaining of pupal retinae with anti-cut antibody and ant-Caz antibody revealed relatively high expression of Caz in cone cells (Fig. 1J) and the Caz signal was reduced by 62% in flies expressing Caz dsRNA drived by *GMR-GAL4* (Fig. 1K and N). Moreover, effective knockdown of *Caz* in pupae of *UAS-Caz-IR*$_{363-399}$ line was demonstrated by the Western immunoblot analysis with anti-*Caz* antibody (Fig. 1O). All of these results further indicate that the rough eye phenotype observed in RNAi flies of *Caz* is due to reduction of the *Caz* protein level.

Knockdown of *Caz* induces apoptosis in pupal retinae

Extensive apoptosis could be considered as one factor causing fused ommatidia in the adult compound eye, since it is frequently accompanies this phenotype. We therefore examined if excessive cell death might occur during eye development in *Caz* knockdown flies by crossing *GMR-GAL4*; *UAS-Caz-IR*$_{363-399}$;+with flies expressing a broad specificity Caspase inhibitor P35 encoded by the baculovirus *Autographa californica* [28]. Partial suppression of the rough eye phenotype induced by knockdown of *Caz* was observed in flies co-expressing P35 (Fig. 2A, a–f). Expression of P35 alone

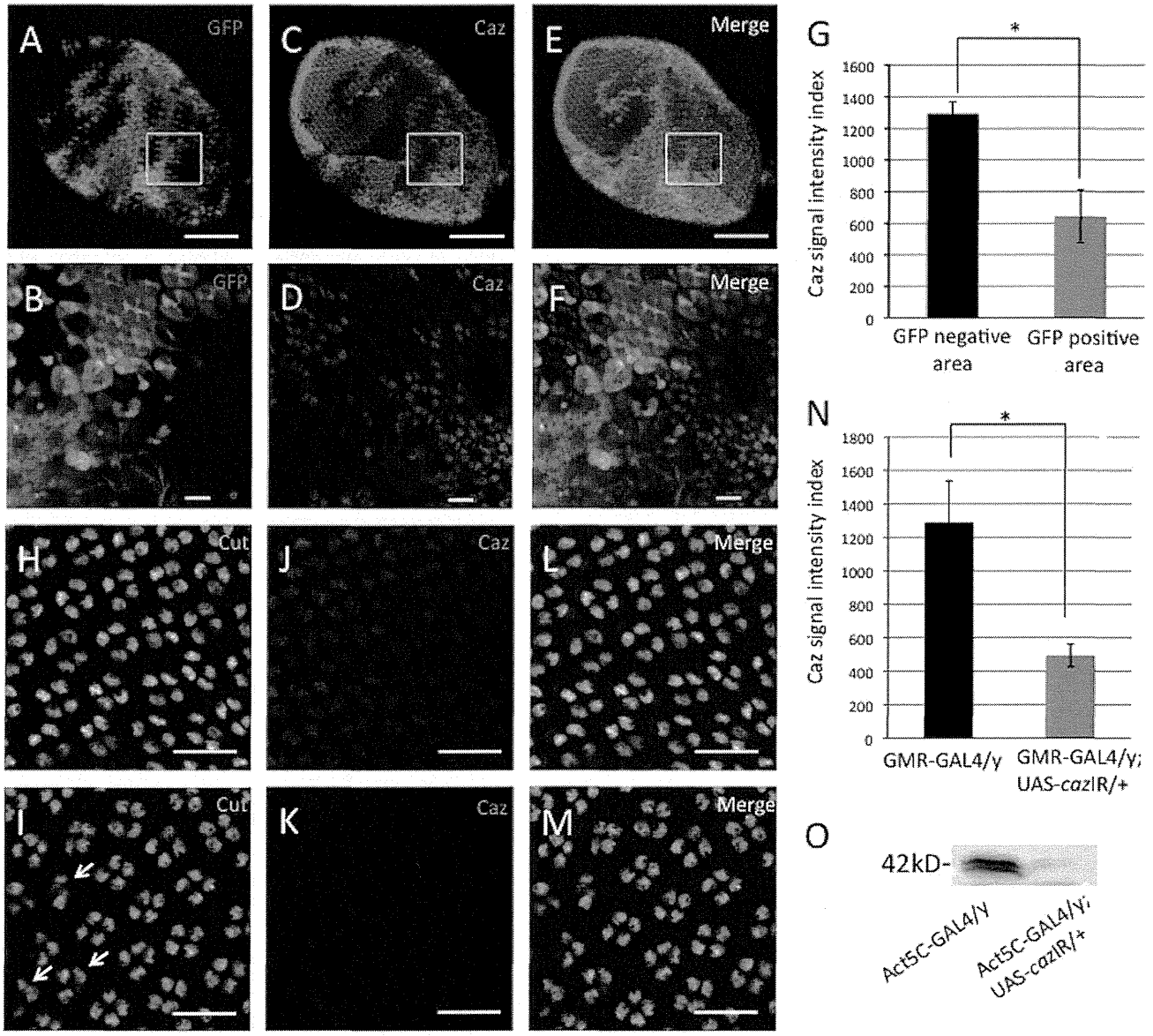

Fig. 1 – The level of anti-*Caz* signals is reduced in *Caz* dsRNA-expressing areas. Immunostaining of retinae for 42 h APF with anti-*Caz* antibody (C, D, J and K). RNAi clones in retinae were generated with the flip-out system (A to F). Female flies with *hspFlp; +; tub*1> *FRT cd2 FRT*> *GAL4, UAS-GFP* were crossed male flies with w; *UAS-Caz-IR*$_{363-399}$; +. The *Caz* dsRNA-expressing area is positively marked with GFP (A, and B). (E and F) Merged images. Panels B, D and F show higher magnification images of the regions marked with squares in panels A, C and D. (G) Quantification of intensities of *Caz*-signals in GFP-positive and –negative areas. Mean intensities with standard deviation from six pupal retinae are shown. *$P<0.05$. (H to M) Immunostaining of retinae for 42 h APF with anti-cut (H and I) and anti-*Caz* (J and K) antibodies. (L and M) Merged images. (H, J and K) *GMR-GAL4/y*. (I, K and M) *GMR-GAL4/y; UAS-Caz-IR*$_{363-399}$. (N) Quantification of intensities of *Caz*-signals. Mean intensities with standard deviation from nine pupal retinae are shown. *$P<0.05$. The bars indicate 100 μm (A, C and E), 10 μm (B, D and F) and 20 μm (H to M), respectively. (O) Western immunoblot analysis. Protein extracts were prepared from the whole pupae of *Drosophila* carrying *Act5C-GAL4/+* (left lane) or *Act5C-GAL4/+; UAS-Caz-IR*$_{363-399}$*/+* (right lane). The blot was probed with anti-*Caz* antibody.

exerted no apparent effect on the compound eye morphology (Fig. 2A, g and h). Moreover, we monitored apoptotic cells in third instar larval eye imaginal discs by TUNEL assay. However, no detectable apoptotic signals in eye imaginal discs of these flies was observed (Fig. 2B, a, d, g and j). We therefore next examined pupal retinae at 42 h APF by TUNEL assay. Apoptotic cells detected in the *Caz* knockdown retinae were significantly reduced in flies expressing P35 (Fig. 2B, c, f and i). These results indicate that knockdown of *Caz* induces apoptosis in some cells in pupal retinae.

Knockdown of *Caz* interferes with cell differentiation in pupal retinae

Photoreceptor cells are known to be generated in a stereotype order: R8 is generated first, with movement posterior from the

morphogenetic furrow, then cells are added pair wise (R2 and R5, R3 and R4, and R1 and R6), and R7 is the last photoreceptor to be added to each cluster [29]. To investigate whether *Caz* knockdown inhibits differentiation of photoreceptor cells, we crossed flies expressing *Caz* dsRNA with two enhancer trap lines, AE127 and P82, to specifically mark photoreceptor cells of R3/R4/R1/R6 and

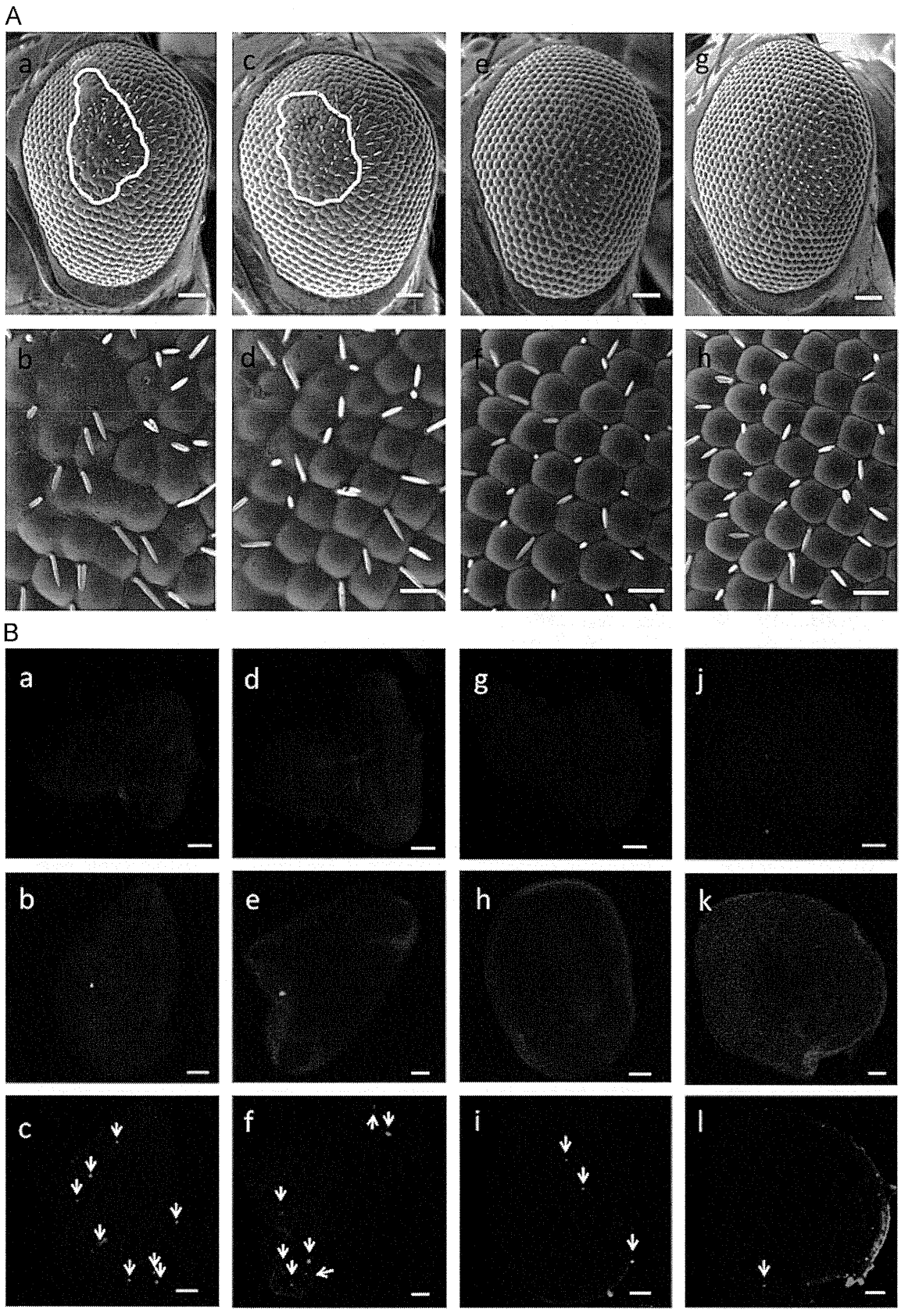

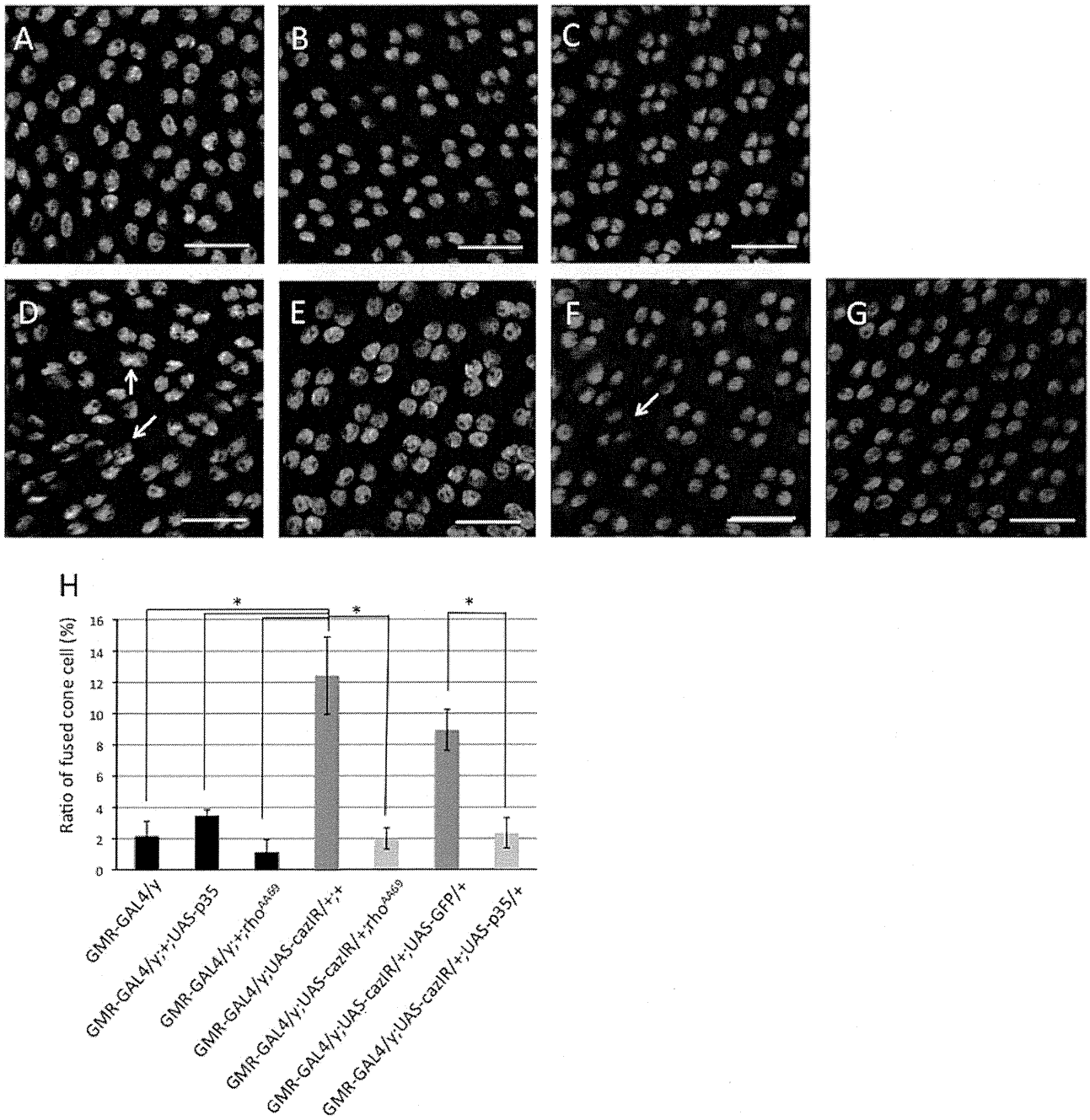

Fig. 3 – Knockdown of *Caz* interferes with differentiation of cone cells. Immunostaining of retinae for 42 h APF with an antibody to Cut that marks cone cells (green). (A) *GMR-GAL4/y*. (B) *GMR-GAL4/y*; +; *UAS-P35*/+. (C) *GMR-GAL4/y*; +; rho^{AA69}/+. (D) *GMR-GAL4/y; UAS-Caz-IR*$_{363-399}$/+; +. (E) *GMR-GAL4/y; UAS-Caz-IR*$_{363-399}$/+; rho^{AA69}/+. (F) *GMR-GAL4/y; UAS-Caz-IR*$_{363-399}$/+; *UAS-GFP*/+. (G) *GMR-GAL4/y; UAS-Caz-IR*$_{363-399}$/+; *UAS-P35*/+. The flies were developed at 28 °C. Arrows show fused cone cells and fused ommatidia are circled. The bar indicates 20 μm (A-G). (H) Quantification of fused cone cells in pupal retinae. Ratio of fused cone cells in each retina us shown (%). Mean values with standard deviation from six pupal retinae are shown. *$P < 0.05$. (Left to Right) *GMR-GAL4/y, GMR-GAL4/y*; +; *UAS-P35*/+, *GMR-GAL4/y*; +; rho^{AA69}/+, *GMR-GAL4/y; UAS-Caz-IR*$_{363-399}$/+; +, *GMR-GAL4/y; UAS-Caz-IR*$_{363-399}$/+; rho^{AA69}/+, *GMR-GAL4/y; UAS-Caz-IR*$_{363-399}$/+; *UAS-GFP*/+ and *GMR-GAL4/y; UAS-Caz-IR*$_{363-399}$/+; *UAS-P35*/+.

Fig. 2 – Knockdown of *Caz* in eye imaginal discs induces apoptosis. (A) Over-expression of P35 suppresses the rough eye phenotype, as shown by scanning electron micrographs of adult compound eyes. (a, b) *GMR-GAL4/y; UAS-Caz-IR*$_{363-399}$/ +; +, (c, and d) *GMR-GAL4/y; UAS-Caz-IR*$_{363-399}$/+; *UAS-GFP*/+, (e, f) *GMR-GAL4/y; UAS-Caz-IR*$_{363-399}$/+; *UAS-P35*/+. (g, and h) *GMR-GAL4/y*; +/+; *UAS-P35*/ +. The flies were developed at 28 °C. The eye phenotype of at least five adult male flies (3 to 5 days old) of each line was examined and the experiments were done in triplicate. No significant variation in eye phenotype was observed among the five individuals. The rough area of the compound eye was circled as an index of the rough eye phenotype. The bars indicate 50 μm(a, c, e and g), and 14.2 μm(b, d, f and h), respectively. (B) Detection of apoptotic cells in third larval eye imaginal discs (a, d, g and j) and pupal retinae (c, f, i and l) by TUNEL assay. Pupal retinae were also stained with DAPI (b, e, h and k). (a to c) *GMR-GAL4/y; UAS-Caz-IR*$_{363-399}$/ +; +. (d to f) *GMR-GAL4/y; UAS-Caz-IR*$_{363-399}$/+; *UAS-GFP*/+. (g to i) *GMR-GAL4/y; UAS-Caz-IR*$_{363-399}$/+; *UAS-P35*/+. (j to l) *GMR-GAL4/y*; +/+; *UAS-P35*/+. The flies were developed at 28 °C. The bars indicate 100 μm.

R3/R4/R7, respectively and then immunostained the eye imaginal discs with anti-β-galactosidase antibodies (Fig. S2, A–B and D–E). In parallel, we carried out immunostaining of eye imaginal discs with anti-Elav antibodies (Fig. S2, C,and F). Elav, a pan-neuronal marker is normally expressed in the posterior portion of the eye imaginal discs. In eye imaginal discs of *Caz* knockdown flies, all eight photoreceptor cells and their neuron appeared to differentiate normally (Fig. S2).

We next examined the pattern formation in pupal ommatidia of *Caz* knockdown flies. Differentiation of photoreceptors, cone cells, and 1°, 2°, and 3° pigment cells was completed by about 42 h APF at 28 °C. However, in pupal retinae of *Caz* knockdown flies, immunostaining with an anti-Cut antibody that marks cone cells showed that some of these were fused in flies expressing *Caz* dsRNA (Fig. 3D and H). Flies carrying *GMR-GAL4* alone exhibited apparently normal cone cells (Fig. 3A and H). The quantified data indicate that occurrence of cone cell fusion was increased by 5.7 fold in the *Caz* knockdown retinae.

Furthermore, we monitored apical cell junctions in pupal retina for 42 h APF by immunostaining with anti-Discs large. The results showed cells in pupal retinae of *Caz* knockdown flies to be attached loosely, the orientation of ommatidia to be irregular, and the size of ommatidia to vary (Fig. 4C). In addition some ommatidia were apparently fused (Fig. 4C). These data suggest that knockdown of *Caz* disrupts differentiation of pupal ommatidial cell types, especially cone cells, and 1°, 2°, and 3° pigment cells, probably by repressing or enhancing expression of genes involved in differentiation processes.

Genetic link between *Caz* and *rhomboid*

The epidermal growth factor-receptor (EGFR) signaling pathway, evolutionarily conserved from *Caenorhabditis elegans* to man, controls a variety of different cellular processes. In *Drosophila*, these include proliferation, patterning, cell-fate determination, migration, and survival [30]. Contributions to cone cell-fate and ommatidial rotation have also been documented [30–33]. One of the rate limiting components of *Drosophila* EGFR signaling is *Rhomboid* [32–34]. We therefore examined the effects of mutations that might modify the Caz-induced rough eye phenotype, especially focusing on the *rhomboid* gene.

Half dose reduction *rhomboid-1* (*rho*) significantly suppressed the rough eye phenotype (Fig. 5A, a, b, c and d) and rescued the fusion of cone cells (Fig. 3E and H) in pupal retinae. Rescue of the fusion of the cone cells was also observed with overexpression of P35 (Fig. 3G and H), suggesting that induction of apoptosis is also responsible for this phenotype. Two different alleles of *rho* showed suppression of the rough eye (Fig. 5A, a, b, c and d). In addition, similar extent of suppression of the rough eye was observed by knockdown of *rho* (Fig. 5A, m and n), but not by expression of dsRNA for GFP (Fig. 5A, k and l). *Rhomboid-1* is a seven membrane-spanning serine protease, undergoing cleavage of Spitz to release the secreted form as an EGFR ligand from the Golgi apparatus [32–35]. In the eye, *Rhomboid-3*, also known as Roughoid, cooperates with *Rhomboid-1* [32,33]. Expectedly, the *Rhomboid-3* hypomorph mutant ru^1 also demonstrated suppression of the rough eye phenotype induced by knockdown of *Caz*

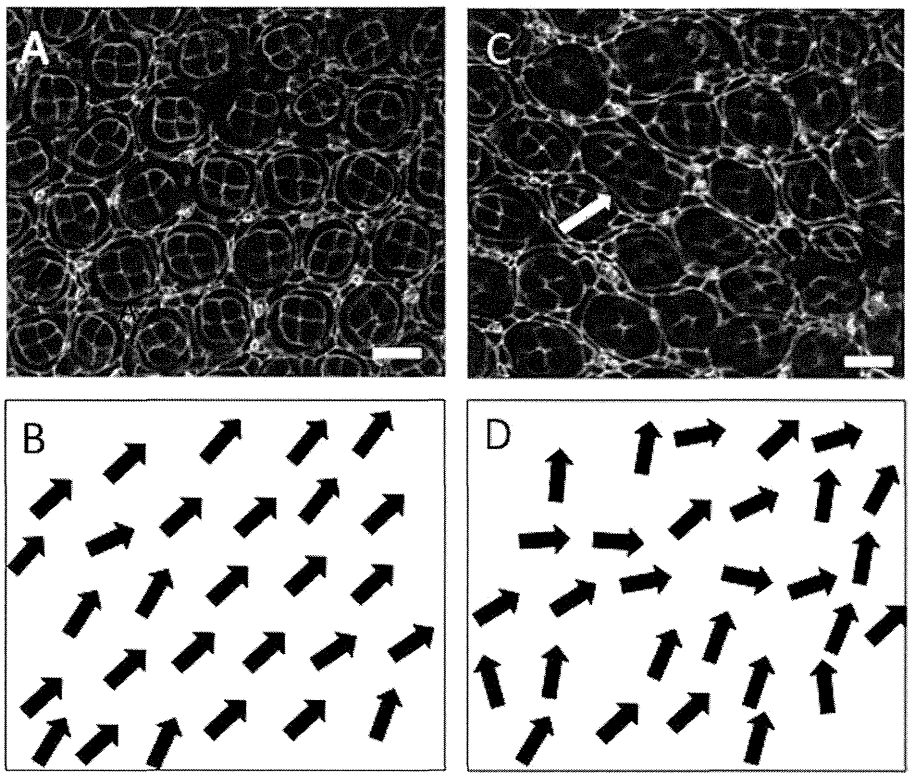

Fig. 4 – Effects of *Caz* knockdown on morphogenesis of pupal retinae. Confocal sections stained with anti-Discs large (A, and C). (A) *GMR-GAL4/y*. (C) *GMR-GAL4/y; UAS-Caz-IR*$_{363-399}$*/+; +*. Black arrows in the lower panels (B, and D) indicate the orientation of the ommatidia. Note disruption in the *Caz* knockdown flies (D) in compared to control (B). The size of ommatidia is also irregular, and cell attachment appears to be loose (compare panels A and C). The white arrow in panel C indicates an example of the fused ommatidia.

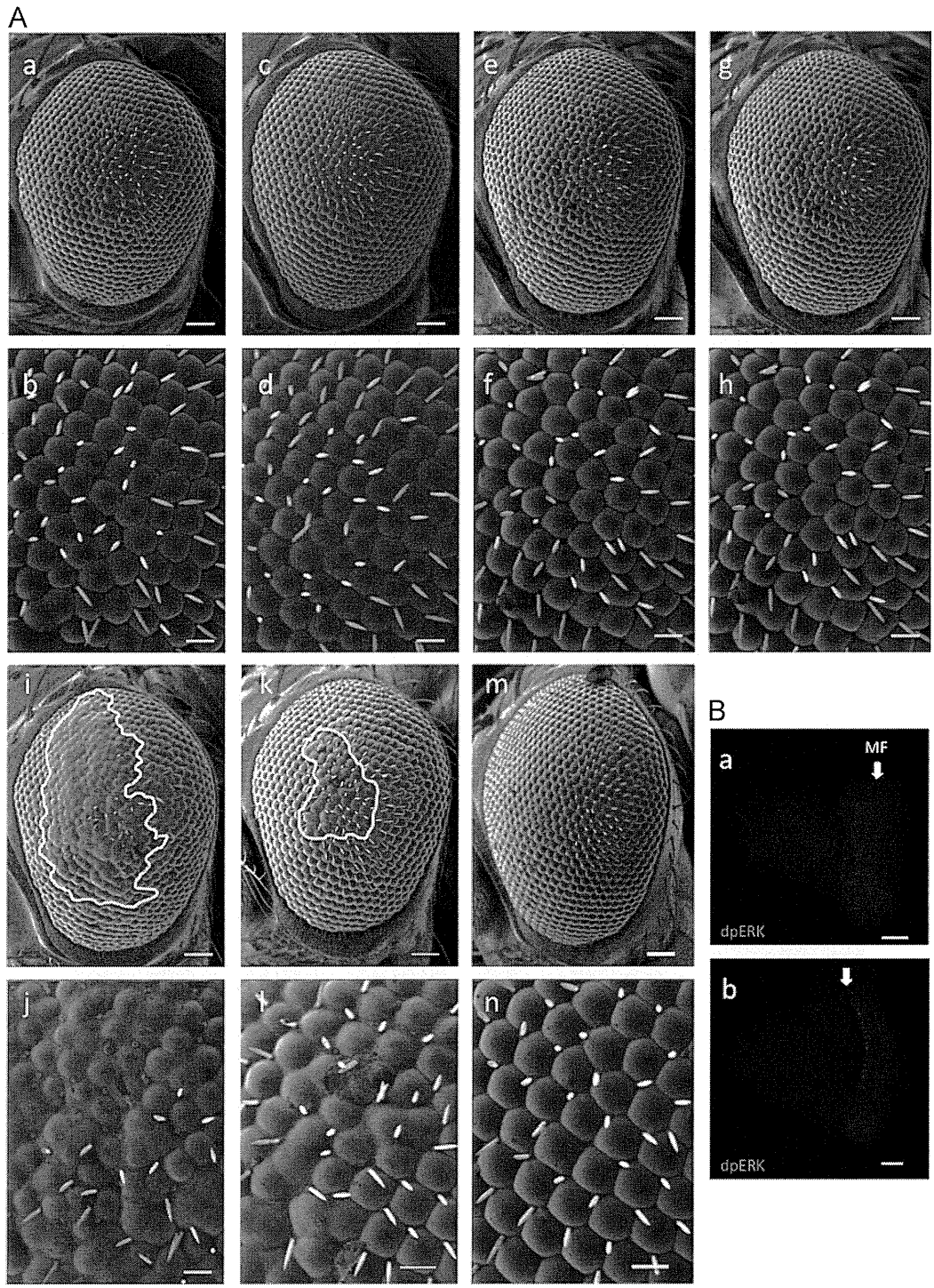

Fig. 5 – Scanning electron micrographs of adult compound eyes. (A) Female flies expressing *Caz* dsRNA (*GMR-GAL4/GMR-GAL4; UAS-Caz-IR*$_{363-399}$; +) were crossed with *UAS-GFP-IR, UAS-rho-IR*^{28690}, *rho*^{7M43} (amorph), *rho*^{4A69} (undetermined), *mirror*^{SaiD3} (loss of function), or *ru*^{1} (hypomorph) male flies, and then F1 progeny were developed at 28 °C without balancer chromosomes and used for inspection of the eye phenotype. The eye phenotype of at least five adult male flies (3 to 5 days old) of each line was examined and the experiments were done in triplicate. No significant variation in eye phenotype was observed among the five individuals. The rough area of the compound eye was circled as an index of the rough eye phenotype. (a, b) *GMR-GAL4/y; UAS-Caz-IR*$_{363-399}$/+; *rho*^{7M43}/+. (c, and d) *GMR-GAL4/y; UAS-Caz-IR*$_{363-399}$/+; *rho*^{4A69}/+. (e, and f) *GMR-GAL4/y; UAS-Caz-IR*$_{363-399}$/ +; *mirror*^{SaiD3}/+(g, and h) *GMR-GAL4/y; UAS-Caz-IR*$_{363-399}$/ +; *ru*^{1}/ +. (i, and j) *GMR-GAL4/ y; UAS-Caz-IR*$_{363-399}$/+; +. (k, and l) *GMR-GAL4/y; UAS-Caz-IR*$_{363-399}$/+; *UAS-GFP-IR*/+, (m, n) *GMR-GAL4/y; UAS-Caz-IR*$_{363-399}$/+; *UAS-rho-IR*^{28690}/+. The flies were developed at 28 °C. The bar indicates 50 μm (a, c, e, g, i, k, and m) or 14.2 μm (b, d, f, h, j, l, and n). (B) Immunostaining of eye imaginal discs with anti-dpERK antibody. (a) *GMR-GAL4/y.* (b) *GMR-GAL4/ y; UAS-Caz-IR*$_{363-399}$/+; +. Arrows indicate morphogenetic furrows (MF). The bars indicate 100 μm.

(Fig. 5A, g and h). Moreover, a *mirror* loss of function mutant $mirr^{SaiD3}$ similarly suppressed the rough eye phenotype (Fig. 5A, e and f). The *mirror* gene encodes a homeodomain-containing transcription factor that is thought to activate transcription of *rhomboid* [36]. In addition, immunostaining of eye imaginal discs with anti-dpERK antibody also pointed activation of ERK signals in the *Caz* knockdown flies (Fig. 5B). These results indicate a genetic link between Caz and the EGFR signaling pathway.

Discussion

In this study, we found that *Caz* knockdown in eye imaginal discs induces a rough eye phenotype associated with apoptosis, abnormal differentiation of cone cells and pigment cells, and defects in ommatidia rotation in pupal retinae. However, apoptosis and differentiation of photoreceptor cells were not affected in larval eye imaginal discs expressing *Caz* dsRNA. Why did *Caz* knockdown in eye imaginal discs affect pupal retinae but not third instar larval eye discs? In situ hybridization and immunohistochemistrical analyses demonstrated that *Caz* mRNA and protein are enriched in the brain and CNS during embryogenesis, and *Caz* protein was detected in the nuclei of several larval tissues and in imaginal discs [21]. However, the expression level of *Caz* is higher in adult eyes than in larval eye discs (Flybase). Thus, it is possible that *Caz* plays a more important role in eye development in the pupal stage.

The observation that the rough eye phenotype of *Caz* knockdown flies was significantly suppressed by co-expression of P35 and that apoptotic cells detected by immunostaining with anti-cleaved Caspase-3 antibody were significantly increased in pupal retinae of flies expressing *Caz* dsRNA suggests that induction of apoptosis at least partially contributes to the rough eye phenotype. It is reported that the number of dying cells increases dramatically if interactions between cells are disrupted, for instance upon cell ablation [37]. Therefore, one possible explanation is that *Caz* knockdown disrupts interactions between cells in pupal retinae, as evidenced with anti-Cut immunostaining, that results in induction of apoptosis. In addition, it is well known that apoptosis is induced by JNK or p38 signaling [38–40]. It is also reported that persistent activation of the JNK or p38 signaling pathways mediates neuronal apoptosis in ALS [3–7,41], and that TDP-43 is related to JNK signaling [42]. Thus, another possible explanation is that *Caz* knockdown induces JNK or p38 signaling, resulting in increase of apoptosis in pupal retinae.

We found a genetic interaction between *Caz* and *Rhomboid*, a rate-limiting component of the EGFR signaling pathway. Appropriate levels of EGFR signaling are required for cone cell-fate and ommatidial rotation [30–33]. Knockdown of *Caz* in eye imaginal discs and pupal retinae induced abnormal differentiation of cone cells and defects in ommatidia rotation that eventually resulted in the rough eye phenotype in adults. The *rhomboid-1* mutant rescued the fusion of cone cells and mutations of *rhomboid-3* and *mirror* significantly suppressed the rough eye phenotype of *Caz* knockdown flies. In contrast, mutations of EGFR did not suppress the rough eye phenotype induced by knockdown of *Caz* (data not shown). These apparently contradictory results might be explained as follows. Once activated, the signaling cascade could be amplified progressively, so that only a half reduction of some components of pathway such as EGFR may not be sufficient to suppress the effects of over-activation of the initiator such as *rhomboid*. In any event, the present study suggests that Caz negatively regulates EGFR signaling. Since the expression level of *Caz* is much higher in adult eyes than larval eye discs, negative regulation of EGFR signaling by *Caz* may play a role in controlling EGFR signaling less reactive to oxidative stress during adulthood. It should be noted that a hallmark of ALS is chronic neuronal exposure to oxidative stress and inflammation.

In summary, we have shown that knockdown of *Caz* in the *Drosophila* retina induces a rough eye phenotype associated with increased apoptosis, abnormal differentiation of cone cells and pigment cells, and defects in ommatidia rotation. Here we provide the first definitive evidence that *Caz* plays an important role in regulation of the EGFR signaling pathway. It should be noted that the neurodegeneration occurring in ALS can be accounted for deviation from strict control of MAPK signaling [3]. Thus, the *Caz* knockdown flies used in the present study should provide a useful tool for elucidating functions of FUS and pathological mechanisms of associated ALS.

Acknowledgments

We thank Dr. Y. Hiromi and Dr. A. Plessis for supplying fly lines, and Dr. M. Moore for comments on the English in the manuscript. This study was partially supported by a scholarship and grants from Japan Science and Technology Agency and the Ministry of Education, Science, Sports and Culture of Japan and the JSPS Core-to-Core Program, B. Asia-Africa Science Platforms.

Appendix A. Supporting information

Supplementary data associated with this article can be found in the online version at http://dx.doi.org/10.1016/j.yexcr.2014.06.004.

REFERENCES

[1] S. Boillee, C. Vande Velde, D.W. Cleveland, ALS: a disease of motorneurons and their nonneuronal neighbors, Neuron 52 (2006) 39–59.
[2] S. Vucic, M.C. Kiernan, Pathology of neurodegeneration in familial amyotrophic lateral sclerosis, Curr. Mol. Med. 9 (2009) 255–272.
[3] E.K. Kim, E.-J. Choi, Pathological roles of MAPK signaling pathways in human diseases, Biochim. Biophys. Acta 2010 (1802) 396–405.
[4] C. Bendotti, M. Bao Cutrona, C. Cheroni, G. Grignaschi, D. Lo Coco, M. Peviani, M. Tortarolo, P. Veglianese, E. Zennaro, Inter- and intracellular signaling in amyotrophic lateral sclerosis: role of p38 mitogen-activated protein kinase, Neurodegener. Dis. 2 (2005) 128–134.
[5] M. Tortarolo, P. Veglianese, N. Calvaresi, A. Botturi, C. Rossi, A. Giorgini, A. Migheli, C. Bendotti, Persistent activation of p38 mitogen-activated protein kinase in a mouse model of familial amyotrophic lateral sclerosis correlates with disease progression, Mol. Cell. Neurosci. 23 (2003) 180–192.
[6] S.S. Holasek, T.M. Wengenack, K.K. Kandimalla, C. Montano, D.M. Gregor, G.L. Curran, J.F. Poduslo, Activation of the stress-activated MAP kinase, p38, but not JNK in cortical motor neurons during early presymptomatic stages of amyotrophic lateral sclerosis in transgenic mice, Brain Res. 1045 (2005) 185–198.

[7] M. Dewil, V.F. dela Cruz, L. Van Den Bosch, W. Robberecht, Inhibition of p38 mitogen activated protein kinase activation and mutant SOD1(G93A)-induced motor neuron death, Neurobiol. Dis. 26 (2007) 332–341.
[8] R. Lemmens, M.J. Moore, A. Al-Chalabi, R.H. Brown Jr., W. Robberecht, RNA metabplism and the pathogenesis of motor neuron diseases, Trends Neurosci. 33 (2010) 249–258.
[9] I.R. Mackenzie, R. Rademakers, M. Neumann, TDP-43 and FUS in amyotrophic lateral sclerosis and frontotemporal dementia, Lancet Neurol. 9 (2010) 995–1007.
[10] M.A. Gitcho, R.H. Baloh, S. Chakraverty, K. Mayo, J.B. Norton, D. Levitch, K.J. Hatanpaa, C.L. White 3rd, E.H. Bigio, R. Caselli, et al., TDP-43 A315T mutation in familial motor neuron disease, Ann. Neurol. 63 (2008) 535–538.
[11] A. Yokoseki, A. Shiga, C.F. Tan, A. Tagawa, H. Kaneko, A. Koyama, H. Eguchi, A. Tsujino, T. Ikeuchi, A. Kakita, et al., TDP-43 mutation in familial amyotrophic lateral sclerosis, Ann. Neurol. 63 (2008) 538–542.
[12] E. Kabashi, P.N. Valdmanis, P. Dion, D. Spiegelman, B.J. McConkey, C. Vande Velde, J.P. Bouchard, L. Lacomblez, K. Pochigaeva, F. Salachas, et al., TARDBP mutations in individuals with sporadic and familial amyotrophic lateralsclerosis, Nat. Genet. 40 (2008) 572–574.
[13] J. Sreedharan, I.P. Blair, V.B. Tripathi, X. Hu, C. Vance, B. Rogelj, S. Ackerley, J.C. Durnall, K.L. Williams, E. Buratti, et al., TDP-43 mutations in familialand sporadic amyotrophic lateral sclerosis, Science 319 (2008) 1668–1672.
[14] G.S. Pesiridis, V.M. Lee, J.Q. Trojanowski, Mutations in TDP-43 link glycine-rich domain functions to amyotrophic lateral sclerosis, Hum. Mol. Genet. 18 (2009) R156–R162.
[15] T.J. Kwiatkowski Jr., D.A. Bosco, A.L. Leclerc, E. Tamrazian, C.R. Vanderburg, C. Russ, A. Davis, J. Gilchrist, E.J. Kasarskis, T. Munsat, et al., Mutations in the *FUS/TLS* gene on chromosome 16 cause familial amyotrophic lateral sclerosis, Science 323 (2009) 1205–1208.
[16] C. Vance, B. Rogelj, T. Hortobagyi, K.J. De Vos, A.L. Nishimura, J. Sreedharan, X. Hu, B. Smith, D. Ruddy, P. Wright, et al., Mutations in *FUS*, an RNA processing protein, cause familial amyotrophic lateral sclerosis type 6, Science 323 (2009) 1208–1211.
[17] C. Hewitt, J. Kirby, J.R. Highley, J.A. Hartley, R. Hibberd, H.C. Hollinger, T.L. Williams, P.G. Ince, C.J. McDermott, P.J. Shaw, Novel *FUS/TLS* mutations and pathology in familial and sporadic amyotrophic lateral sclerosis, Arch. Neurol. 67 (2010) 455–461.
[18] R. Rademakers, H. Stewart, M. Dejesus-Hernandez, C. Krieger, N. Graff-Radford, M. Fabros, H. Briemberg, N. Cashman, A. Eisen, I.R. Mackenzie, *Fus* gene mutations in familial and sporadic amyotrophic lateral sclerosis, Muscle Nerve 42 (2010) 170–176.
[19] H. Zinszner, J. Sok, D. Immanuel, Y. Yin, D. Ron, *TLS* (*FUS*) binds RNA in vivo and engages in nucleo-cytoplasmic shuttling, J. Cell Sci. 110 (1997) 1741–1750.
[20] C. Lagier-Tourenne, M. Polymenidou, D.W. Cleveland, TDP-43 and *FUS/TLS*: emerging roles in RNA processing and neurodegeneration, Hum. Mol. Genet. 19 (2010) R46–R64.
[21] D.T. Stolow, S.R. Haynes, Cabeza, a *Drosophila* gene encoding a novel RNA binding protein, shares homology with EWS and TLS, two genes invoved in human sarcoma formation, Nucleic Acids Res. 23 (1995) 835–843.
[22] H. Sasayama, M. Shimamura, T. Tokuda, Y. Azuma, T. Yoshida, T. Mizuno, M. Nakagawa, N. Fujikake, Y. Nagai, M. Ymaguchi, Knockdown of the *Drosophila* Fused in Sarcoma (*FUS*) homologue causes deficient locomotive behavior and shortening of motoneuron terminal branches, PLoS One 7 (2012) e39483.
[23] M. Mlodzik, Y. Hiromi, U. Weber, C.S. Goodman, G.M. Rubin, The *Drosophila seven-up* gene, a member of the steroid receptor gene superfamily, controls photoreceptor cell fates, Cell 60 (1990) 211–224.
[24] S. Kramer, S.R. West, Y. Hiromi, Cell fate control in the *Drosophila* retina by the orphan receptor *seven-up*: its role in the decisions mediated by the ras signaling pathway, Development 121 (1995) 1361–1372.
[25] Y. Takahashi, F. Hirose, A. Matsukage, M. Yamaguchi, Identification of three conserved regions in the DREF transcription factors from *Drosophila melanogaster* and *Drosophila virilis*, Nucleic Acids Res. 27 (1999) 510–516.
[26] J. Sun, J. Tower, FLP recombinase-mediated induction of Cu/Zn superoxide dismutase transgene expression can extend the life span of adult Drosophila melanogaster, Mol. Cell. Biol. 19 (1999) 216–228.
[27] Y. Azuma, T. Tokuda, M. Shimamura, A. Kyotani, H. Sasayama, T. Yoshida, I. Mizuta, T. Mizuno, M. Nakagawa, N. Fujikake, M. Ueyama, Y. Nagai, M. Yamaguchi, Identification of *ter94*, *Drosophila VCP*, as a strong modulator of motor neuron degeneration induced by knockdown of *Caz*, *Drosophila FUS*, Hum. Mol. Genet. 23 (2014) 3467–3480.
[28] N.E. Crook, R.J. Clem, L.K. Miller, An apoptosis-inhibiting baculovirus gene with a zinc finger-like motif, J. Virol. 67 (1993) 2168–2174.
[29] S.L. Zipursky, G.M. Rubin, Determination of neuronal cell fate: lessons from the R7 neuron of *Drosophila*, Annu. Rev. Neurosci. 17 (1994) 373–397.
[30] K. Gaengel, M. Mlodzik, EGFR signaling regulates ommatidial rotation and cell motility in the *Drosophila* eye via MAPK/Pnt signaling and the Ras effector Canoe/AF6, Development 130 (2003) 5413–5423.
[31] W. Fu, M. Noll, The *Pax2* homolog sparkling is required for development of cone and pigment cells in the *Drosophila* eye, Genes Dev. 11 (1997) 2066–2078.
[32] J.D Wasserman, S. Urban, M. Freeman, A family of rhomboid-like genes: *Drosophila rhomboid-1* and *roughoid/rhomboid-3* cooperate to activate EGF receptor signaling, Genes. Dev. 14 (2000) 1651–1663.
[33] B.Z. Shilo, Regulating the dynamics of EGF receptor signaling in space and time, Development 132 (2005) 4017–4027.
[34] S. Yogev, E.D. Schejter, B.Z. Shilo, *Drosophila* EGFR signaling is modulated by differential compartmentalization of Rhomboid intramembrane proteases, EMBO J. 27 (2008) 1219–1230.
[35] S. Urban, J.R. Lee, M. Freeman, *Drosophila* rhomboid-1 defines a family of putative intramembrane serine proteases, Cell 107 (2001) 173–182.
[36] K.C. Jordan, N.J. Clegg, J.A. Blasi, A.M. Morimoto, J. Sen, D. Stein, H. McNeill, W.M. Deng, M. Tworoger, H. Ruohola-Baker, The homeobox gene *mirror* links EGF signalling to embryonic dorsoventral axis formation through notch activation, Nat. Genet. 24 (2000) 429–433.
[37] A. Hidalgoa, C.F. Constant, The control of cell number during central nervous system development in flies and mice, Mech. Dev. 120 (2003) 1311–1325.
[38] F. Agnè, M. Suzanne, S. Noselli, The *Drosophila* JNK pathway controls the morphogenesis of imaginal discs during metamorphosis, Development 126 (1999) 5453–5462.
[39] M. Tare, R.M. Modi, J.J. Nainaparampil, O.R. Puli, S. Bedi, P. Fernandez-Funez, M. Kango-Singh, A. Singh, Activation of JNK signaling mediates amyloid-β-dependent cell death, PLoS One 6 (2011) e24361.
[40] S.A. Correa, K.L. Eales, The role of p38 MAPK and its substrates in neuronal plasticity and neurodegenerative disease, J. Signal. Transduct 2012 (2012) 649079.
[41] S. Ackerley, A.J. Grierson, S. Banner, M.S. Perkinton, J. Brownlees, H.L. Byers, M. Ward, P. Thornhill, K. Hussain, J.S. Waby, B.H. Anderton, J.D. Cooper, C. Dingwall, P.N. Leigh, C.E. Shaw, C.C. Miller, p38α stress-activated protein kinase phosphorylates neurofilaments and is associated with neurofilaments pathology in amyotrophic lateral sclerosis, Mol. Cell. Neurosci. 26 (2004) 354–364.
[42] J. Meyerowitz, S.J. Parker, L.J. Vella, D.Ch. Ng, K.A. Price, J.R. Liddell, A. Caragounis, Q.X. Li, C.L. Masters, T. Nonaka, M. Hasegawa, M.A. Bogoyevitch, K.M. Kanninen, P.J. Crouch, A.R White, C-Jun N-terminal kinase controls TDP-43 accumulation in stress granules induced by oxidative stress, Mol. Neurodegener. 6 (2011) 57.

INTERNAL MEDICINE

□ CASE REPORT □

Hereditary Diffuse Leukoencephalopathy with Spheroids Characterized by Spastic Hemiplegia Preceding Mental Impairment

Fukiko Kitani-Morii[1], Takashi Kasai[1], Kei Tomonaga[1], Kozo Saito[1], Ikuko Mizuta[1], Akira Yoshioka[2], Masanori Nakagawa[1,3] and Toshiki Mizuno[1]

Abstract

Hereditary diffuse leukoencephalopathy with spheroids (HDLS) is a young-adult-onset autosomal dominant white matter disease characterized by progressive cognitive dysfunction. We herein report the case of a 20-year-old woman who developed spastic hemiplegia. Brain magnetic resonance imaging revealed increased bilateral T2 signal intensity and bright diffusion-weighted imaging signals with a low apparent diffusion coefficient within the frontoparietal white matter. The lesion gradually expanded for over one year. The patient was initially diagnosed with multiple sclerosis (MS); however, she did not respond to immunosuppressive therapy. DNA sequencing showed a heterozygous c.2381T>C mutation in colony-stimulating factor 1 receptor. HDLS with a pure motor phenotype is sometimes difficult to differentiate from MS.

Key words: hereditary diffuse leukoencephalopathy with spheroids, CSF1R mutation, multiple sclerosis, diffusion-weighted image, apparent diffusion coefficient

(Intern Med 53: 1377-1380, 2014)
(DOI: 10.2169/internalmedicine.53.1932)

Introduction

Hereditary diffuse leukoencephalopathy with spheroids (HDLS) is a young-adult-onset autosomal dominant white matter disease characterized by progressive cognitive dysfunction, behavioral changes, motor impairment and seizures (1). The diagnosis is usually made following a brain biopsy or autopsy based on the presence of neurodystrophy and large areas of neuroaxonal swelling known as spheroids (2). After several mutations in *colony-stimulating factor 1 receptor* (*CSF1R*) were recently shown to underlie HDLS (3), various clinical courses and imaging features of the disease were revealed through genetic diagnosis. We herein report a case of HDLS with progressive spastic hemiplegia that was initially diagnosed as multiple sclerosis (MS).

Case Report

A 20-year-old left-handed Japanese woman was admitted to our neurological department due to progressive right spastic hemiplegia that had started five months before admission. The patient's development was normal and her previous medical history was unremarkable, including neither head trauma nor seizures. She had no history of drug abuse, including alcohol. She had been a good volleyball player while a student, and after graduating from high school, she enrolled in nursing school. Her mother had a 10-year history of cognitive decline that had progressed until she became functionally mute with a diagnosis of frontotemporal dementia at 40 years of age. Her maternal grandmother died in her 40s, and she had a younger brother who exhibited no mental or physical problems.

Upon admission, the patient was alert and oriented, with a

[1]Department of Neurology, Graduate School of Medical Science, Kyoto Prefectural University of Medicine, Japan, [2]Department of Clinical Research, National Hospital Organization Maizuru Medical Center, Japan and [3]North Medical Center, Kyoto Prefectural University of Medicine, Japan

Received for publication October 17, 2013; Accepted for publication December 23, 2013

Correspondence to Dr. Fukiko Kitani-Morii, f-morii@koto.kpu-m.ac.jp

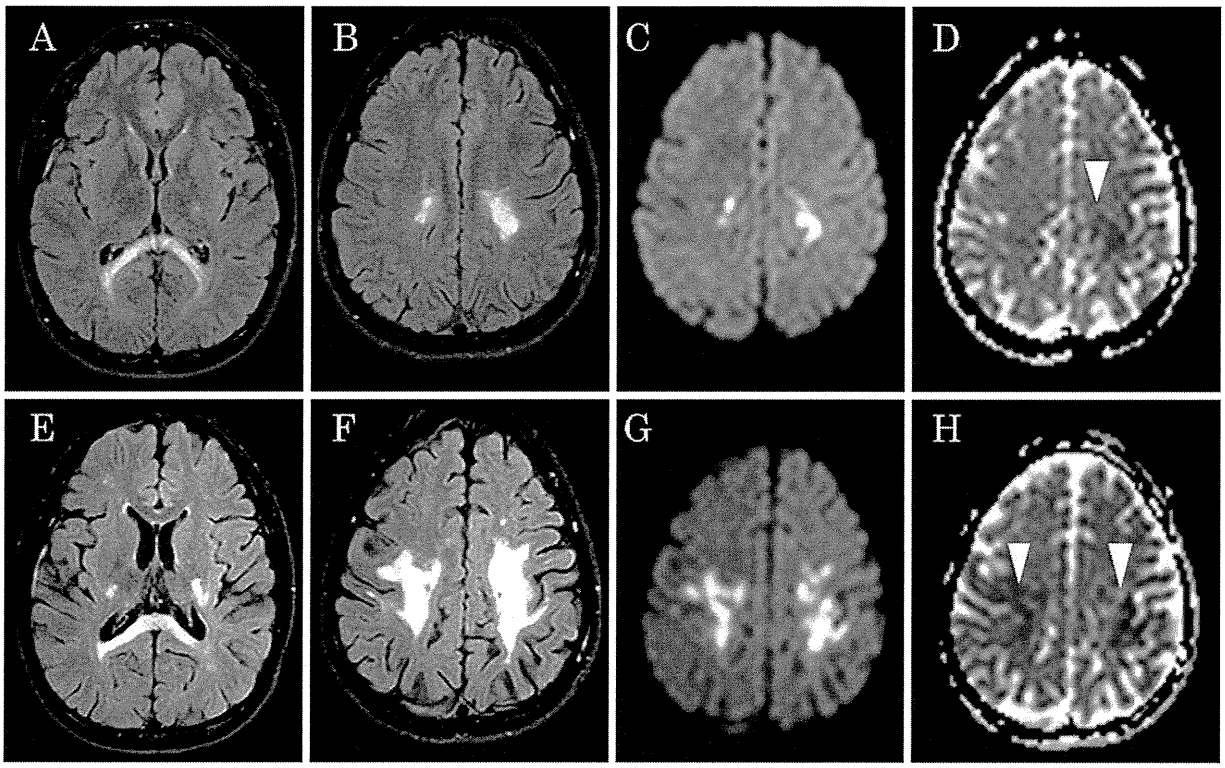

Figure 1. **Neuroimaging findings. Brain MR images at the first admission are shown in the upper row (A-D). (A) (B) FLAIR images show increased intensity in the corpus callosum, pyramidal tract, and frontoparietal white matter. (C) Bright DWI and (D) low ADC were observed in the areas of FLAIR signal abnormalities (arrowheads). The bottom row (E-H) shows MR images obtained 1 year later in which signal abnormalities were more extensive. FLAIR: fluid-attenuated inversion recovery, DWI: diffusion-weighted image, ADC: apparent diffusion coefficient**

full Mini-Mental State Examination score. The general findings were unremarkable. A neurological examination showed slight spasticity, motor weakness, sensory loss, exaggerated deep tendon reflexes and an extensor plantar response in the right extremities. She had no visual or urinary problems. Routine laboratory findings were unremarkable. Tests with negative or normal results were as follows: anti-nuclear antibodies, HIV, soluble interleukin-2 receptor, angiotensin-converting enzyme, anti-aquaporin 4 antibodies, very long chain fatty acids, arylsulfatase A and a cerebrospinal fluid (CSF) analysis, including myelin basic protein, oligoclonal bands and the IgG index. The activity of galactocerebrosidase was slightly low, although not significantly. An aerobic exercise test showed a slight increase in the levels of lactate and pyruvate. A nerve conduction study, electroencephalogram and visual evoked potential were normal.

Brain magnetic resonance imaging (MRI) revealed bilateral, but left dominant, increased T2 and fluid-attenuated inversion recovery (FLAIR) signal intensity within the frontoparietal white matter, corticospinal tract and splenium of the corpus callosum (Fig. 1A, B). The arcuate fasciculus was spared. Bright diffusion-weighted image (DWI) signals and a low apparent diffusion coefficient (ADC) were recognized in the areas of T2/FLAIR signal abnormalities, except for the brainstem (Fig. 1C, D). No post-gadolinium enhancement was noted. ^{18}F-fluorodeoxy glucose positron emission tomography (PET) showed no abnormal uptake in these areas. MRI of the spine was normal. N-isopropyl-^{123}I-p-iodoamphetamine single photon emission computed tomography imaging revealed substantial left dominant decreases in flow in the frontoparietal white matter. Magnetic resonance angiography was completely normal.

The patient's clinical course and radiological features suggested MS, except for the absence of CSF abnormalities. She was tentatively diagnosed with MS on the first admission and treated with intravenous and oral corticosteroids and plasmapheresis without benefit.

At the one-year follow-up visit, the patient was wheelchair-bound and demonstrated worsened right spastic hemiplegia as well as a slight cognitive decline, emotional incontinence, dysarthria and spasticity on the left side. Brain MRI disclosed enlarged bilateral white matter lesions with increased T2/FLAIR signal intensity, bright DWI and low ADC (Fig. 1E-H).

After providing genetic counseling for the patient and her father, we obtained their informed consent and extracted genomic DNA from peripheral blood leukocytes obtained from the patient and her parents using an ABI 3130 Genetic Analyzer (Applied Biosystems, Foster City, USA), and exons 12-22 of *CSF1R* were amplified with polymerase chain reaction (PCR). A direct sequence analysis of the PCR-amplified DNA revealed a heterozygous c.2381T>C muta-

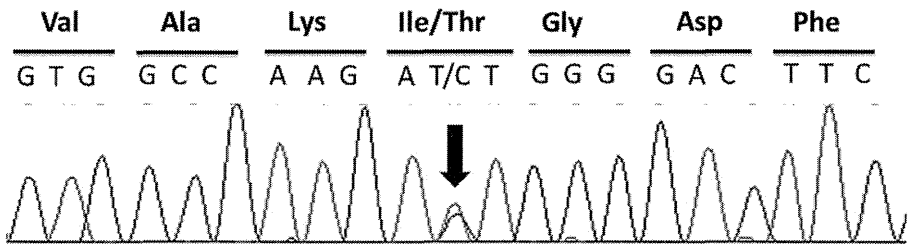

Figure 2. DNA sequencing findings. A heterozygous c. 2381T>C mutation in exon 18 of CSF1R was identified in this patient (arrow). CSF1R: colony-stimulating factor 1 receptor

tion in exon 18 in the patient and her mother (Fig. 2). This mutation has previously been reported in patients with HDLS (3).

Discussion

We herein reported a case of HDLS in which a diagnosis of MS was initially considered due to the patient's young age, subacute progressive spastic hemiplegia and white matter lesions.

The initial symptoms of HDLS typically include cognitive dysfunction and personality changes, accompanied by motor impairment, including weakness, spasticity, rigidity, tremors and seizures (1). HDLS patients are frequently misdiagnosed with Alzheimer's disease, frontotemporal dementia, atypical parkinsonism and other leukoencephalopathy syndromes, such as adrenoleukodystrophy, metachromatic leukodystrophy and Krabbe disease (1, 4, 5).

The primary symptoms in this case were subacute and progressive motor impairment without cognitive decline, which are common clinical features of MS in young women. In fact, the patient's clinical course (one year of disease progression) and radiological findings (evidence of lesion dissemination in the space in the brain based on T2-weighted images in at least one area characteristic of MS, e.g., periventricular, juxtacortical or infratentorial) satisfied the McDonald criteria for primary progressive MS, except for the absence of CSF abnormalities (6). Moreover, the differential diagnosis of white matter lesions and callosal lesions, including neuromyelitis optica, progressive multifocal leukoencephalopathy (PML), Marchiafava disease and adrenoleukodystrophy, was unlikely taking into consideration the patient's clinical history and laboratory data. In contrast to the patient, her mother primarily exhibited cognitive decline and was diagnosed with frontotemporal dementia, which is retrospectively consistent with the typical symptoms of HDLS. However, we initially did not regard the mother's symptoms to be related to the patient's disease due to the phenotypic differences.

Case reports regarding a pure motor type of HDLS have recently accumulated (7-9). Discriminating between HDLS and MS is often difficult, especially in such cases. As seen in the present patient and her family, the clinical phenotype of HDLS, including the initial symptoms and age of onset, vary considerably, even the pedigree. Inheritance in patients with HDLS may be concealed by such clinical heterogeneity. In fact, patients with HDLS are sometimes found to have sporadic disease (7, 10). The heritability of MS, on the other hand, has been established, such that the presence of genetic factors increases the risk of developing MS; the age-adjusted risk of recurrence in offspring is 2.07 (95%CI 1.41-2.73) (11). These facts suggest that the presence of neurological disorders in relatives does not provide sufficient evidence to discriminate between MS and HDLS. Appropriate comprehension of HDLS is required to make a correct and rapid diagnosis using genetic analyses, which should also be helpful for avoiding unnecessary treatment, including immunosuppressive therapy, for the pure motor type of HDLS, as observed in the present case.

Generally, the brain MRI findings of HDLS patients show white matter lesions that are hyperintense on T2-weighted and FLAIR images and hypointense on T1-weighted images unaccompanied by contrast uptake (12). Bifrontoparietal areas of T2/FLAIR hyperintensity are often asymmetric, especially in the early stage of the disease. The presence of lesions in deep, subcortical and periventricular areas is typical, with occasional involvement of the corticospinal tract and corpus callosum (12). Most of the MRI abnormalities observed in our case, including the presence of T2/FLAIR abnormalities in periventricular lesions, the corticospinal tract and the corpus callosum without contrast enhancement, are compatible with the well-documented radiological characteristics of this disease.

Previous authors have reported restricted diffusion in areas with corresponding dark ADC values in patients with HDLS (10, 13-16), while few cases of HDLS with restricted diffusion persisting over a long period, as observed in the present patient, have been documented. Mateen et al. reported one case of HDLS in which bright DWI with dark ADC values persisted for 19 weeks, and a brain biopsy revealed advanced axonal loss with spheroid formation, myelin loss and gliosis. The authors speculated that the restricted diffusion of extracellular water is associated with the presence of degraded myelin sheaths (14). Sundal et al. described the case of a patient who was followed with MRI for 16 months after disease onset, which revealed initially high signal intensity on DWI with restricted mean diffusivity. In that case, the high signal area on DWI and restricted diffusivity changed dynamically throughout the follow-up period. After the lesion reached the peripheral rim of the